University of Alberta

Fabrication of WC-based Metal Matrix Composite Coatings via Low-pressure Cold Spraying for Enhanced Surface Properties

by

Natanael Manuel Melendez

A thesis submitted to the Faculty of Graduate Studies and Research
in partial fulfillment of the requirements for the degree of

Master of Science

Department of Mechanical Engineering

Fall 2013
Edmonton, Alberta

Abstract

A low-cost, low-pressure cold spray unit was used to fabricate tungsten carbide (WC)-based metal matrix composite (MMC) coatings. A variety of coatings were fabricated and characterized. Scanning electron microscopy (SEM), coupled with image analysis, Vickers micro-hardness, and X-ray diffraction (XRD) were used to characterize the coatings. Image analysis was used to determine the WC content in the coatings and the mean free path between the reinforcing particles. The WC content in the coating increased as the WC content in the powder blend increased. As the WC content in the powder increased, the coating porosity decreased and the WC deposition efficiency increased. ASTM standard G65-2004 dry abrasion testing was conducted on WC-Ni coatings to determine a relationship between hardness and wear resistance. A linear relationship was observed between the wear rate and hardness of the WC-Ni MMC coatings. The coating deemed optimal had a wear rate comparable to those of WC-Co coatings fabricated by high-velocity oxy-fuel (HVOF) and high-pressure cold spraying.

Acknowledgements

I would like to start with thanking my supervisor, Dr. André McDonald. Without his support and guidance during my graduate studies this thesis would not be possible. Although I was always pushed to the limit during my graduate studies, it was an enjoyable two years and I have gained a lot of knowledge and experience. I would also like to thank Dr. Gary Fisher for the fruitful discussions at Alberta Innovates – Technology Futures. I would like to thank both of them for teaching engineering principles as well as professionalism.

I would also like to thank everyone in the workshop for assisting me during my graduate studies. In particular, I would like to thank Roger Marchand and Dave Waege for their assistance and patience while fixing the cold spray torch. That experience allowed me to become more familiar with the cold spray torch and gave me excellent "hands-on" experience. I would also like to thank Shiraz Merali and Diane Caird for conducting XRD tests on my samples. I would like to thank De-ann Rollings, Nathan Gerein, and George Braybrook for the countless hours I spent with them obtaining SEM images. Finally, I would like to thank Hoa Dang at Alberta Innovates – Technology Futures for conducting the numerous wear tests needed for this thesis.

I would like to thank everyone from Room 6-25. I would like to thank Navid Pourjavad and Shishir Rao for mentoring me during my undergrad and early stages of my masters. I would like to personally thank David Therrien, Erik

Sullivan, Rael Gonzalez, and Greg Nelson for the interesting conversations inside and outside of the office to keep me sane. I would like to thank Vinayak Narulkar for the insightful discussions about wear. Lastly, I would like to mention that I am appreciative for the cultural diversification in Room 6-25; I enjoyed learning about different cultures.

I would like to thank all my friends for being there for me. In particular, I would like to thank Brian Claypool and Avviene Aquino for being supportive of my decision and having me over for countless dinners. I would like to thank Ian Smith for getting me out of the office during the nice summer days for lunch.

Last, but certainly not the least, I would like to thank my family for being supportive of my decision and encouraging me to advance my education. I would also like to thank my mother, whose everlasting love has motivated me to complete my work and has made me who I am today. I know she would be proud of this accomplishment and I am forever grateful for how she and my grandparents raised me.

Table of Contents

List of Tables

List of Figures

Nomenclature and Abbreviations

i. List of Symbols

f	Volume fraction (vol.%)
H	Hardness (HV)
$\overline{H}$	Effective hardness (HV)
m	Mass (g)
N_L	Number of particle intercepts per unit length of test line (μm^{-1})
P	Applied load (N)
s	Sliding distance (m)
Δv	Volume loss (mm^3)
V_P	Volume fraction of the reinforcing particles (vol.%)
W	Wear rate (mm^3/Nm)

ii. Greek Symbols

λ	Mean free path between the reinforcing particles (μm)

iii. Subscripts

CS	Coated substrate
FPB	Final mass of powder blend
h	Hard phase
Lower	Lower limit
OPB	Original mass of powder blend
S	Substrate
s	Soft phase
Upper	Upper limit

v. List of Abbreviations

Al	Aluminum
Al_2O_3	Alumina
APS	Air Plasma Spray
BSE	Backscattered Electron
Cr^{6+}	Hexavalent Chromium
Cu	Copper
DE	Deposition Efficiency

Fe	Iron
EDS	Energy Dispersive X-ray Spectroscopy
FMR	Flow Meter Reading
FSP	Friction Stir Processing
HVOF	High Velocity Oxy-fuel Spray
MMC	Metal Matrix Composite
Ni	Nickel
p	Pure
PTA	Plasma Transfer Arc
ROM	Rule of Mixtures
SCFH	Standard Cubic Feet per Hour
SE	Secondary Electron
SEM	Scanning Electron Microscope
WC	Tungsten Carbide
WC-Co	Tungsten Carbide-cobalt Cermet
XRD	X-ray Diffraction
YSZ	Yttria Stabilized Zirconia

1. Introduction

1.1 WC-Co Cermets

Tungsten carbide-cobalt (WC-Co) cermets are well known for their unique combination of hardness and toughness, which yields excellent wear resistance. Sintered WC-Co hard-metals have been used in aggressive wear environments and due to the environmental restrictions of hexavalent chromium (Cr^{6+}) ions, WC-Co coatings have become very popular as an alternative [1, 2]. Although thermal-sprayed WC-Co coatings do not provide the same properties as their sintered counterparts, they do have comparable properties if the appropriate thermal spray process and parameters are used [3]. Furthermore, Houdková *et al*. [2] have shown that thermal-sprayed tungsten carbide (WC)-based coatings can outperform other coatings, such as NiCrBSi, Cr_2O_3, and Cr_3C_2-NiCr, which can be used for wear application. However, the wear performance is dependent on the type of test used. For example, dry or wet three-body abrasion, sliding wear, or erosion, and the type of cermet must be carefully selected and the carbide size, powder size, feedstock composition, and process parameters must be optimized to achieve the desirable wear properties for application.

1.2 Thermal Spraying

Thermal spraying is a common method used for coating materials to enhance their surface properties. Thermal spraying is a process that melts and accelerates powder particles towards a prepared substrate to fabricate a coating [4]. Thermal spraying can deposit metal, ceramic or polymer materials onto a variety of metal, ceramic or polymer substrates [5]. Several common processes include air plasma spray (APS), high-velocity oxy-fuel (HVOF) spraying, flame spraying, and cold gas dynamic spraying (cold spraying), where each process has a unique combination of both temperature and velocity. Figure 1 [4 - 6] compares the ranges of both the process temperature and the velocities of each process discussed. The figure shows that the operating temperatures of the APS process are on the order of 8,000 to 14,000°C, while for cold spraying the operating temperatures are on the order of 25 to 600°C. Furthermore, operating temperatures must be lower than the melting temperature of the feedstock powder because it is a solid-state process. Due to the lower temperatures, high particle velocities (~300 – 1800 m/s) are required to deposit a coating using cold spraying.

APS uses a plasma generator that consists of an anode and a cathode. The torch is continuously cooled with water to prevent torch damage. Argon is used as the primary gas to stabilize the torch, while hydrogen, helium, nitrogen, or a combination of these are used as a secondary gas to generate a plasma and enhance heat transfer to the particles [4]. The powder can be fed radially or axially. Due to the high temperature of the plasma plume, this process is ideal for

the deposition of ceramics such as yttria-stabilized zirconia (YSZ). Flame and HVOF spraying are similar in the sense that they both combust a hydrocarbon fuel in oxygen to generate a flame. However, HVOF spraying accelerates particles to high speeds (up to 2000 m/s) in comparison to flame spraying (up to 50 m/s). This is attributed to the high pressure of the combustion gas inside the mixture chamber [4]. Due to the increased particle velocities, coatings fabricated by HVOF typically have lower coating porosities in comparison to other high temperature thermal spray processes. Due to these features, flame spraying and HVOF spraying can be used to deposit some ceramics, metals and cermets (a ceramic-metal compound). Furthermore, in industrial practice, HVOF spraying is typically used to fabricate carbide hard-metals (such as WC-Co).

Cold spraying, which is a relatively novel thermal spray process, accelerates small (1 – 50 μm) metal or alloy particles to high velocities (300 – 1800 m/s) at temperatures significantly lower than their melting point to fabricate thick, dense, adherent coatings [7]. The high velocities are obtained by compressing the working fluid to high pressures. Furthermore, the velocity of the working fluid is increased by using a de Laval nozzle. The processing gases employed are typically helium, nitrogen, or air [4]. The high velocity of the gases increases the velocities of the particles, promoting bonding through adiabatic shear instabilities at the interface of the particle and substrate during particle plastic deformation [8 - 12]. The low processing temperatures minimizes or eliminates phase transformations, porosity, and residual stresses, which is prominent in high temperature thermal spray processes. Phase transformations or chemical changes

can introduce brittle phases which have undesirable mechanical properties, such as higher wear rates. Figure 2 shows a generic schematic of the cold spray process [13]. The figure shows that the pressurized processing gas is heated up to a desired temperature, while the powder is fed through a separate gas line. The two lines are mixed together at either the converging or diverging section of the de Laval nozzle [14]. Finally the particles fabricate a coating via plastic deformation. The cold spray process can be separated into two different categories: high-pressure and low-pressure cold spraying. Cold spraying at high pressure typically employs a working fluid at pressures in excess of approximately 2 MPa [15 - 20], while cold spraying at low pressure typically uses a working gas at pressures below 1 MPa (150 psig) [12, 21 - 28]. Due to these features, cold spraying is typically used to fabricate metal or metal alloy coatings because metal or metal alloys are easier to deform plastically. However, high pressure cold spraying can be used to deposit harder particles because higher particle velocities can be achieved. Recently low-pressure cold spraying has been used to fabricate metal matrix composite (MMC) coatings [21 - 28].

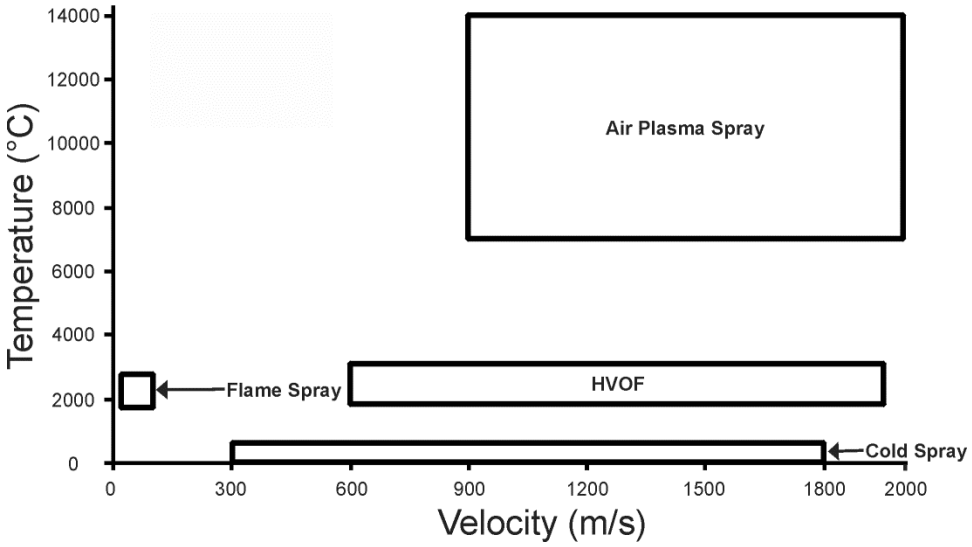

Figure 1: Typical range of flame temperatures and velocities for a variety of thermal spray processes [4 - 6]

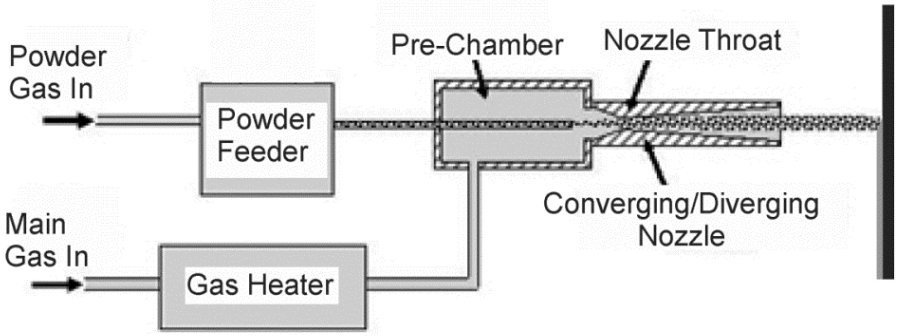

Figure 2: General schematic of the cold spray process [13]

Thermal-sprayed coatings are used in a variety of applications because they offer improved wear resistance, corrosion resistance, dimensional control and restoration, heat transfer (conductivity and resistance), and electrical properties, or a combination of any of the aforementioned surface properties.

To take advantage of the material properties of the feedstock powder, cold spraying was chosen because phase transformations, chemical changes, residual stresses, and porosity are minimized, if not eliminated, in these coatings due to the low processing temperatures and high velocities [7]. However, due to the hard nature of WC-Co particles, a softer powder must be added to facilitate deposition.

1.3 Background

1.3.1 Thermal-sprayed WC-based Coatings

WC-based MMC coatings are very useful in aggressive wear environments due to their unique combination of hardness and toughness. These coatings are often preferred over their bulk counterparts because it is often more feasible to coat a prepared part than it is to prepare and machine a bulk WC-Co cermet. Typically, high temperature processes such as HVOF spraying and plasma transfer arc (PTA) overlaying are used to fabricate WC-based MMC coatings to enhance the surface properties of the work piece for various applications [2, 3, 29 - 48]. However, these high temperatures can lead to phase transformations, chemical changes, residual stresses, and porosity. The most common chemical change observed in WC-based MMC coatings is decarburization [29 - 31]. Guilemany *et al*. [29] observed that the WC particles in the agglomerated WC-Co particles can decompose into W_2C by oxidation in the flame. Furthermore, it was observed that complex secondary phases can be formed when the cobalt binder was melted in the flame. Secondary phases that contain both tungsten and carbon in the cobalt

matrix can be present in HVOF-sprayed WC-Co coatings [29]. Studies have shown that an increase in decarburization will decrease the abrasion resistance of the WC-based coating because it introduces undesirable brittle phases [31, 36]. Although the presence of these phases increases the hardness of the fabricated coating, they ultimately decrease its longevity. The WC-Co (or iron [Fe] or nickel [Ni]) pseudo phase diagram [49] and tungsten-carbon (W-C) phase diagram [50] (Figs. 3 and 4, respectively) suggest that decarburization or any other phase transformation should not occur below a temperature of approximately 1250°C. Furthermore, it has been suggested that the solubility of W and C are similar in cobalt and nickel matrices [51].

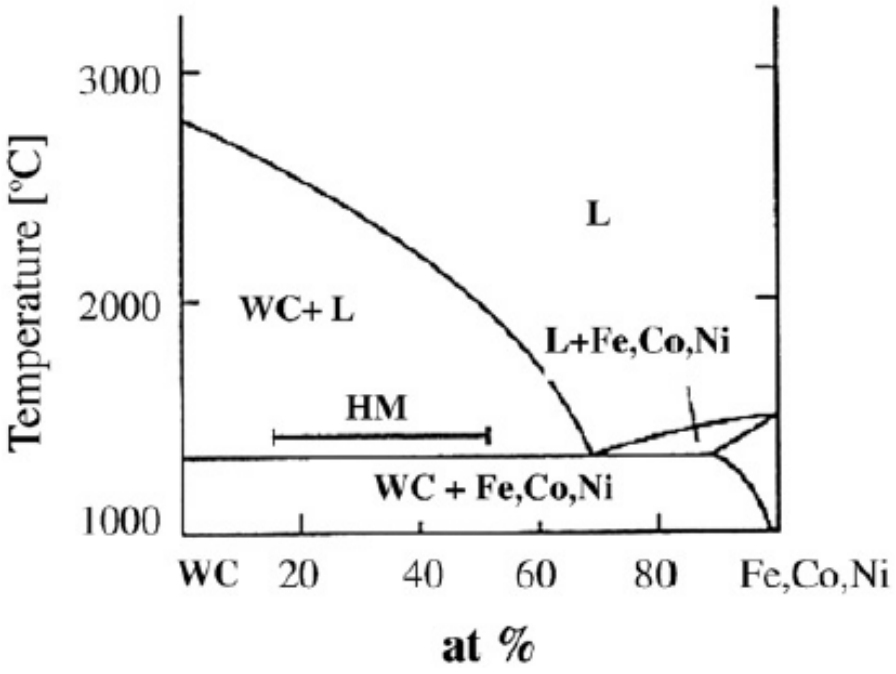

Figure 3: WC-Co pseudo phase diagram [49]

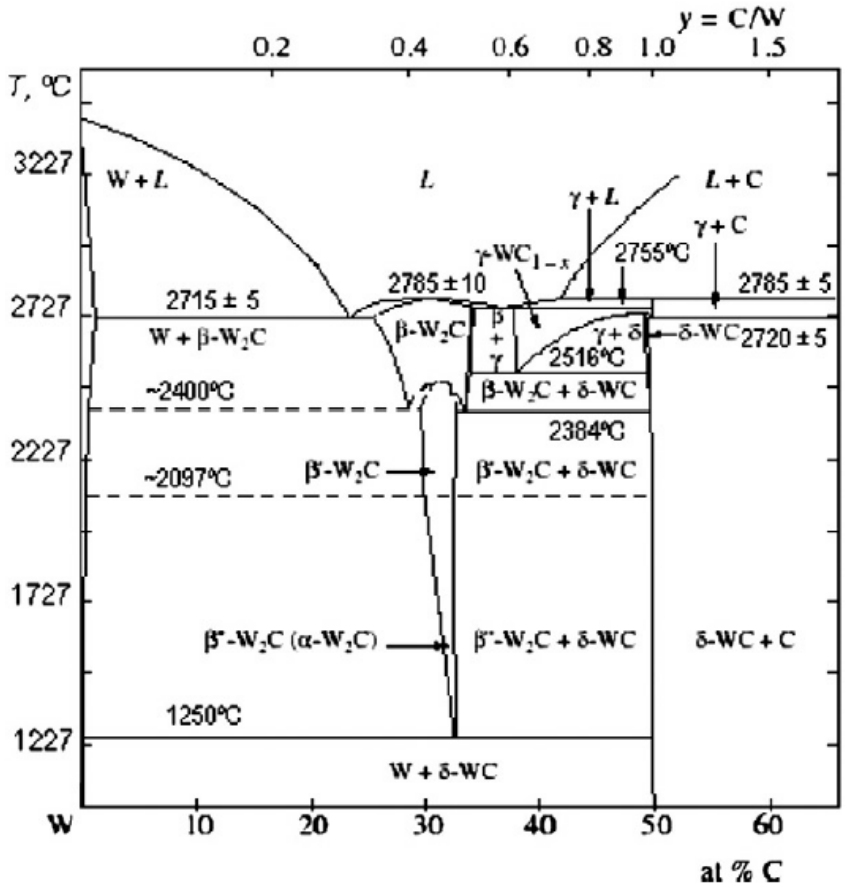

Figure 4: W-C phase diagram [50]

Other forms of thermal spraying have been used to fabricate WC-Co cermet coatings. APS has been used to fabricate WC-Co cermet coatings; however, the WC-Co particles experience more decarburization due to the higher plasma plume temperature and the greater amount of time spent in the plume in comparison to HVOF spraying [52 - 55]. Along with higher levels of decarburization in comparison to other thermal spray processes, the fabricated WC-Co coatings generally have higher coating porosities and increased residual stresses that can cause cracking parallel and perpendicular to the splat boundaries. This contributes to a lower wear resistance, when compared to HVOF-sprayed WC-Co coatings.

However, recent studies have shown that if helium is used instead of hydrogen as the secondary gas, the WC-Co particles experience less decarburization, yielding improved wear properties [54, 55]. A modified version of HVOF spraying, also known as warm spraying, has been developed by mixing nitrogen with the flame in a mixing chamber to decrease the temperature of the flame. Studies have shown that it is possible to fabricate coatings using warm spray with mechanical properties comparable to HVOF-sprayed WC-based coatings with minimal decarburization [56, 57].

To eliminate decarburization completely, cold gas dynamic spraying or "cold spraying" has been used to fabricate WC-based MMC coatings [15 - 21]. Lima *et al*. [15] fabricated thin nanostructured WC-12Co coatings using high-pressure (2 MPa) cold spraying with nitrogen as the processing gas at a temperature of 540°C. It was found that WC-12Co particles could plastically deform the substrate to form a thin coating that was much denser than the original feedstock powder. The low porosity of the coating yielded higher hardness values than the original feedstock powder. Gao *et al*. [16] also determined that it was difficult to build thick WC-based coatings using high-pressure cold spraying with helium at 650°C. When more than one pass was used to fabricate the coating, deposition became challenging because it was difficult for the accelerated WC-Co particles to deform onto the previously deposited WC-Co layer.

Kim *et al*. [17] successfully fabricated thick WC-Co coatings by high-pressure cold spraying, by pre-heating the powder to 200 – 500°C and operating the nozzle at higher pressures on the order of 3 – 4.4 MPa. The high-pressure cold spray

system used either nitrogen or helium as the processing gas. They were able to fabricate coatings with average hardness values of 918 – 2053 $HV_{0.5}$, which is comparable to or exceeds the hardness of typical HVOF-sprayed WC-12Co coatings. Gao *et al*. [18] also fabricated thick nanostructured WC-12Co coatings by high-pressure cold spraying of nanostructured powder with varying feedstock porosity. It was observed that the hardness of the coatings were approximately 2000 $HV_{0.3}$. Dosta *et al*. [19] successfully fabricated WC-25Co cermet coatings using high-pressure cold spraying with nitrogen as the processing gas. They were able to fabricate coatings with hardness values of approximately 800 – 1000 $HV_{0.3}$. None of the high-pressure cold-sprayed coatings exhibited evidence of decarburization.

While previous studies have shown that it is possible to fabricate WC-based coatings with high-pressure cold spraying, relatively few investigators have explored the fabrication of WC-based MMC coatings using a cold spray unit operated at low pressure. Wang and Villafuerte [21] fabricated WC-based MMC coatings using a cold spray unit operating at low pressure. They fabricated coatings using two different types of powder systems. The WC particles were either mechanically blended with copper or aluminum powder or the WC particles were coated with copper or aluminum. The coating that obtained the highest hardness was fabricated using 20 wt.% copper coated WC (WC-20Cu) powder. The hardness of the coating was approximately 200 HB.

Although limited work has been conducted on the fabrication of WC-based MMC coatings using low-pressure cold spraying, other studies have successfully

fabricated other types of MMC coatings using low-pressure cold spraying [22 - 28]. In particular, Spencer *et al*. [26] experimentally determined that the ceramic (alumina) content in fabricated MMC coatings is usually lower than the ceramic content in the powder. The alumina content in the coating was lower because it is very difficult for alumina particles to adhere to the substrate and previously deposited layers of coating due to its inability to deform plastically.

1.3.2 Wear of WC-based MMCs

The evaluation of hardness is a common method used to characterize the quality and to predict the wear resistance of a material or coating. However, hardness is not the sole indicator of a material's ability to withstand wear. Studies have shown that hardness, along with toughness, accurately describes how a coating will perform in a wear environment [3, 44, 58, 59]. Other studies have shown that hardness has a more prominent effect on the wear resistance of a material over toughness [42, 60], while other studies have shown that the wear resistance of a material can be linearly proportional to hardness [58, 61]. Therefore, in order to compare different materials or materials fabricated by different processes, the wear rate or wear resistance must be determined.

Wayne and Sampath [3] compared the wear resistance of sintered bulk WC-Co cermets to WC-Co coatings that were fabricated using different high-temperature thermal spray techniques. It was found that HVOF-sprayed WC-Co coatings had an abrasion resistance that outperformed other high-temperature thermal spraying processes and was similar to that of sintered WC-Co. Numerous studies have been

conducted on WC-based MMC coatings deposited via high-temperature processes, primarily HVOF spraying, to evaluate their wear performance through 3-body abrasion [2, 31, 35 - 43, 46], erosion [2, 3, 32, 44], sliding wear [2, 32, 33, 40, 41], and micro-scale abrasion [34, 45] tests. Stewart *et al*. [31] showed that minimizing decarburization produced an improvement in wear resistance of the coatings. Even though cold spraying has been shown to produce no evidence of WC decarburization in the coatings, a limited amount of work is available on the wear rate of cold-sprayed WC-based MMC coatings. Dosta *et al*. [19] conducted ASTM standard G65-2004 dry abrasion wear tests on high-pressure cold-sprayed WC-25Co coatings and found that the wear resistance of the WC-25Co coatings was lower than that which is typical of HVOF-sprayed WC-Co coatings. Although the cold-sprayed coatings did not undergo decarburization, the higher cobalt content in the feedstock powder and the resultant coating, ultimately induced higher wear rates of the fabricated MMC coating.

Although there are limited published results available on the wear resistance of WC-based MMC coatings fabricated using low-pressure cold spraying, there have been some studies conducted on the characterization of low-pressure cold-sprayed MMC coatings. Irissou *et al*. [23] deposited aluminum-alumina (Al-Al_2O_3) MMC coatings via low-pressure cold spraying and found that when the alumina content in the coating increased, an increase in hardness was observed. However, there was no significant improvement in the abrasion resistance of the coating. Spencer *et al*. [26] fabricated Al-Al_2O_3 MMC coatings using a cold spray variant known as kinetic metallization. The process gas was compressed to 620 kPa. It was found

that an increased amount of alumina (up to 75 vol.%) in a pure aluminum matrix improved the wear resistance significantly, while only a small amount of alumina (25 vol.%) was required to improve the wear resistance of the MMC coating drastically, when 6061 aluminum alloy was used as the matrix. Further increases in alumina content showed no improvement in the wear resistance of the MMC coating.

1.3.3 Mean Free Path of Reinforcing Particles

The inclusion of hard phase reinforcing materials into MMC coatings will increase the strength of the coating. The strengthening effects are typically attributed to the mean free path between the reinforcing particles. Kouzeli and Mortensen [62] showed that the mean free path directly influenced the mechanical properties of MMC's. The mean free path has been used to describe the improvement of mechanical properties for WC-based coatings [35, 36, 48]. A decrease in mean free path yields an improvement in the mechanical properties of the coating, which motivates the fabrication of WC-based MMC coatings from agglomerated WC-based powders that contain small carbides. Studies have shown that coatings fabricated with nano-agglomerated particles possess improved mechanical properties compared to those fabricated from conventional powders [63, 64]. However, high-temperature spray processes were used, which required careful optimization of the spray parameters to ensure that a bimodal microstructure of embedded solid nano-particles in the coating was obtained [31].

1.4 Objectives

The overall objective of this study was to develop a hard-faced WC-based MMC coating using a low-cost, low-pressure cold spray unit. To accomplish this goal the following objectives were met:

1. Optimization of the cold spray parameters and mechanical blend compositions to deposit coatings with a thickness of at least 300 μm successfully using the least amount of torch passes.
2. Identification of the materials present in the sprayed coating through Scanning Electron Microscopy (SEM) coupled with Energy Dispersive X-ray Spectroscopy (EDS). The phases were also confirmed using X-ray Diffraction (XRD).
3. Determination of the relation between the WC content in the mechanical powder blend and the fabricated coating.
4. Quantification of the hardness of the WC-based MMC coatings fabricated from the various mechanical blends through and relate the hardness to the WC content in the coating.
5. Application of the WC-Ni MMC coatings to ASTM G65-2004 dry abrasion tests.
6. Determination of the relation between the coating hardness and the wear rate of the coating, as well as relate the properties through accepted theory.
7. Comparison of the WC-Ni MMC coatings to WC-based MMC coatings fabricated using pure WC particles.

1.5 Thesis Organization

This thesis document is divided into several chapters. Chapter 2 describes the experimental method used to fabricate and characterize the cold-sprayed WC-based MMC coatings. Chapter 3 presents the results and analysis of the experiments conducted on the coatings. Chapter 4 presents the conclusions of this study, while Chapter 5 will discuss the future work for this study.

2. Experimental Method

2.1 Powder and Substrate

A variety of WC-based mechanical blends were explored in this study to fabricate WC-based MMC coatings via low-pressure cold spraying. As a preliminary test, a spray-dried agglomerated WC-10 wt.% Ni-2 wt.% Cu (referred to as "WC-10Ni-2Cu" as a powder and "WC" when mixed with the nickel and copper powders to form a blend and coating) powder was used in an attempt to fabricate a WC-based MMC coating. The spray-dried agglomerated WC-10Ni-2Cu (Pacific Particulate Materials Ltd., Port Moody, BC, Canada) powder had a size distribution of -45+20 μm (20 to 45 μm). However, due to the hard nature of the powder and to facilitate deposition, the WC-10Ni-2Cu powder was mechanically blended with nickel (SST-N5001, Centerline, Ltd., Windsor, ON, Canada) and copper (KSF-C22843, Centerline, Ltd., Windsor, ON, Canada) powders that were specially designed for low-pressure cold spraying. Figure 5 shows the morphology of the WC-10Ni-2Cu, nickel, and copper powders, respectively. The WC-10Ni-2Cu particles are spherical in shape, while the nickel and copper particles have an irregular shape. Table 1 provides the compositions of the WC-Ni-Cu mechanical blends. The various mechanical powder blends were cold-sprayed onto low carbon steel substrates for characterization, which had dimensions of 13 mm x 13 mm x 3mm (0.5 in x 0.5 in x 0.125 in). The substrates

were roughened using #24 alumina grit medium (Manus Abrasive Systems, Inc., Edmonton, AB, Canada) to promote adhesion of the final coating.

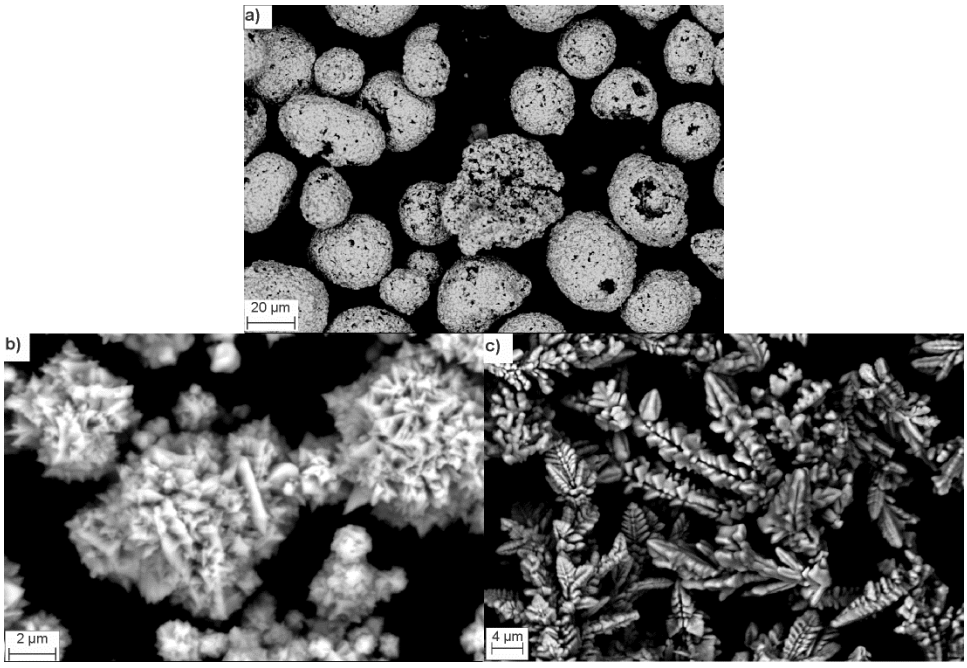

Figure 5: Morphology of *a*) Spray-dried agglomerated WC-10wt.% Ni-2 wt.% Cu powder, *b*) nickel, and *c*) copper powder

Table 1: Composition of WC-10Ni-2Cu based mechanical blends

Mechanical blend	**WC-10Ni-2Cu (wt.%)**	**Ni (wt.%)**	**Cu (wt.%)**
35WC-30Ni-35Cu	35	30	35
88WC-10Ni-2Cu	88	10	2
92WC-6Ni-2Cu	92	6	2
96WC-2Ni-2Cu	96	2	2

Also, a sintered and crushed WC-12 wt.% Co (referred to as "WC" when mixed with nickel powder to form a blend and coating) powder (72F-NS, Sulzer Metco, Westbury, NY, USA), with a size distribution of -45+15 µm, was mechanically blended with the specially designed nickel powder for cold spraying to fabricate the WC-Ni MMC coatings. Figure 6 shows the morphology of the

WC-based powder, which has an irregular shape. The morphology of the nickel powder was the same as the nickel powder used to fabricate the WC-Ni-Cu MMC coatings. The compositions of each mechanical blend and the nickel control powder are presented in Table 2. The various mechanical powder blends were cold-sprayed onto low carbon steel substrates for characterization and dry abrasion testing. The substrates used for characterization had dimensions of 13 mm x 13 mm x 3mm (0.5 in x 0.5 in x 0.125 in), while the dimensions of the substrates used for the dry abrasion testing were 76 mm x 25 mm x 13 mm (3 in x 1 in x 0.5 in). The substrates were roughened using #24 alumina grit medium to promote adhesion of the final coating.

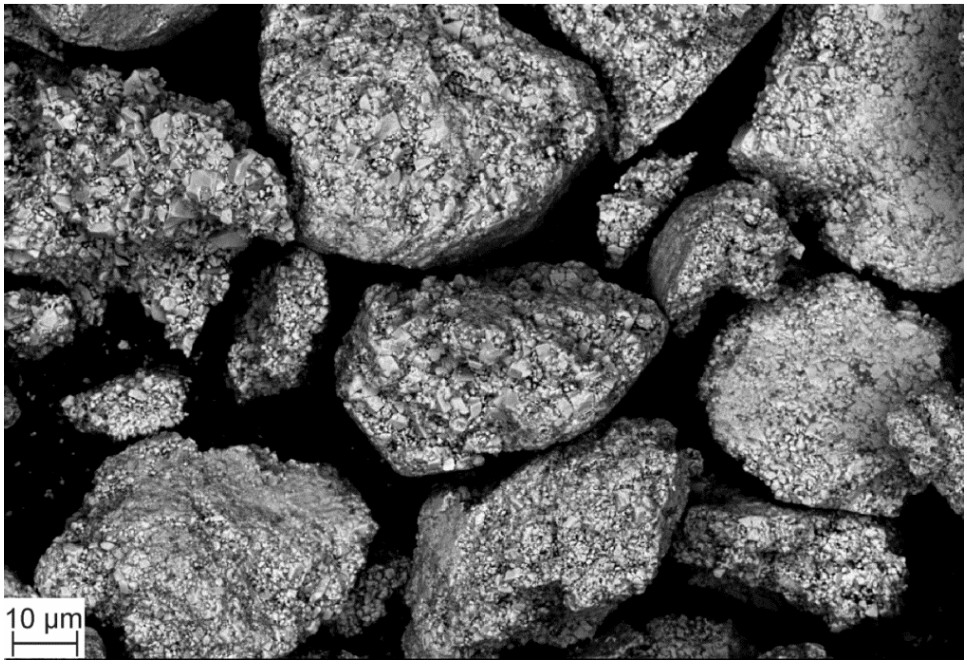

Figure 6: Morphology of WC-12 wt.% Co powder

Table 2: Composition of WC-12wt. % Co based mechanical blends

Mechanical blend	WC-12 wt. % Co (wt.%)	Ni (wt.%)
50WC-50Ni	50	50
75WC-25Ni	75	25
92WC-8Ni	92	8
96WC-4Ni	96	4

A pure WC powder (WCIV, Buffalo Tungsten, Depew, NY, USA) with a size distribution of -50+25 μm was mechanically blended with the same nickel powder used to facilitate deposition of the WC-12 wt.% Co particles. Figure 7 shows the morphology of the WC powder. The particles are irregular with rounded edges. This mechanical blend system and the resulting MMC coatings were fabricated to compare to the WC-Ni coating system described above. Therefore, a mechanical blend composition of 96 wt.% WC + 4 wt.% Ni was used as a starting point because that composition fabricated coatings with the highest WC content. However, higher WC composition blends (98 wt.% WC + 2 wt.% Ni and 99 wt.% WC + 1 wt.% Ni) were explored and successfully deposited onto substrates with dimensions of 13 mm x 13 mm x 3mm (0.5 in x 0.5 in x 0.125 in). The substrates were roughened using #24 alumina grit medium to promote adhesion of the final coating. To avoid confusion between the two WC-Ni systems, MMC coatings fabricated using pure WC particles will be denoted as p-WC+Ni, where ‘p’ represents pure.

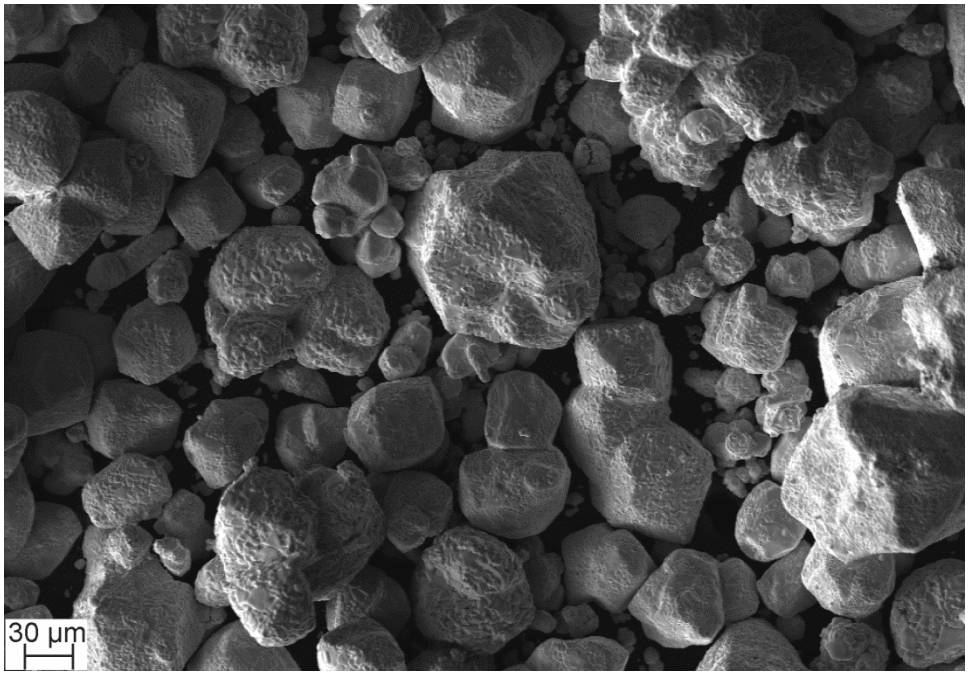

Figure 7: Morphology of pure WC powder

2.2 Cold Spray Deposition

A cold spray system operated at low pressure (SST series P, CenterLine, Ltd., Windsor, ON, Canada) was used to deposit the different mechanical powder blends. Compressed air was used as the working fluid. The cold spray nozzle was attached to a robot (HP-20, Motoman, Yaskawa Electric Corp., Waukegan, IL, USA) for automatic control. A nozzle with a length of 120 mm, an entrance diameter of 4.46 mm, and an exit diameter of 6.40 mm was used to transport the powder and the compressed air from the de Laval nozzle to the substrate. A volumetric powder feeder (5MPE, Sulzer Metco, Westbury, NY, USA), using argon as the carrier gas, was used to transport the powder blend to the nozzle and increase the particle velocities at impact. The cold spray parameters were

optimized to deposit WC-Ni-Cu mechanical blends and then modified to successfully deposit the WC-Ni mechanical blends and are presented in Table 3.

Table 3: Cold spray parameters used to deposit the mechanical powder blends

Parameters	**WC-Ni-Cu powder blends**	**WC-Ni powder blends**
Pressure of compressed air (psig)	88	92
Temperature of compressed air (ºC)	475	550
Stand-off distance (mm)	5	5
Nozzle velocity (mm/s)	5	5
Pressure of argon carrier gas (psig) for the powder	70	70
Volumetric flow rate of argon carrier gas (SCFH) for the powder	15	15
FMR (flow meter reading) of the powder	60	60

2.3 Characterization and Microstructural Analysis

The coated substrates were cold-mounted in an epoxy resin (LECO, Mississauga, ON, Canada) for microstructural analysis. Each cold-mounted specimen was ground using 180, 400, 800, and 1200 grit paper (LECO, Mississauga, ON, Canada) and polishing was conducted with a 1 μm diamond slurry (LECO, Mississauga, ON, Canada) as the final step.

A sputter coater (EM SCD 005, Leica [Baltec Instrument], Balzers, Liechtenstein) with a carbon evaporation accessory was used to deposit a thin carbon coating onto the cold-mounted samples to prevent sample charging in the scanning electron microscope (SEM). A SEM (EVO MA 15, Zeiss, Cambridge, UK) equipped with energy-dispersive X-ray spectroscopy (EDS) was used to analyze the cross-sectional microstructure of the coatings and to determine the

chemical composition of the coatings. Images of the cross-section were captured using the backscattering electron (BSE) and secondary electron (SE) mode.

An image analysis software program (ImagePro, Media Cybernetics, Bethesda, MD, USA), coupled with the SEM micrographs, was used to estimate the WC content in the coatings as well as the mean free path between the reinforcing particles. Lower magnifications of the images were chosen because the entire cross-section had to be analyzed due to the non-homogeneous distribution of the WC reinforcing particles. For the preliminary study of the WC-Ni-Cu coatings, three images were used to determine the average WC content (in vol.%) in the coating. For the WC-Ni coatings, at least nine images of each coating system were used to determine the average WC content (in vol.%). The Count/Size function in the ImagePro software was used to quantify the WC content. The intensity range used was very close to the intensity range of "automatic bright objects" in order to obtain consistent WC content measurements. There were minor deviations from that intensity range because all the WC particles were not captured by ImagePro when selecting the "automatic bright objects" feature. The porosity of each MMC coating and the control coatings was also determined using the image analysis software. For the preliminary study of the WC-Ni-Cu coatings, at least three images were used to determine the porosity of the WC-Ni-Cu coatings and the copper and nickel control coatings. At least nine images of the WC-Ni MMC coating and three images of the nickel control coatings were used to estimate the porosity of the coatings.

The measure distance function, available in ImagePro, was used to estimate the mean free path of the WC reinforcing particles for both the WC-Ni and p-WC+Ni MMC coatings. A random line was drawn on the image and the number of times the line intersected a WC particle was recorded. This was completed for a total of 45 times on multiple images. ImagePro presents the length of the line in pixels. Therefore, a line was used to measure the scale bar to convert pixels into micrometers. The number of particle intercepts per unit length of test line (N_L) and the volume fraction of the reinforcing particles (V_P) was used to determine the mean free path (λ) between the reinforcing particles, according to the following equation [48, 62]:

$$\lambda = \frac{1 - V_P}{N_L}. \quad (1)$$

2.4 Micro-hardness

A micro-Vickers hardness indenter (MVK-H1, Mitutoyo, Aurora, IL, USA) was used to measure the overall hardness of the coatings. For the WC-Ni-Cu and WC-Ni coatings, at least forty five (n = 45) indentations were conducted on the coatings fabricated by each mechanical powder blend system, where fifteen micro-hardness indentations were conducted on each coating sample. Thirty (n = 30) and forty five (n = 45) indentations were conducted on the control coatings for the WC-Ni-Cu (nickel and copper) and the WC-Ni (nickel) coating systems, respectively. Each control coating had fifteen micro-hardness indentations conducted on them. Finally, twenty (n = 20) indentations were conducted on the

various p-WC+Ni coatings, where ten micro-hardness indentations were conducted on each fabricated coating. Each indentation was formed by a 300 gf load for a dwell time of 10 s. Standard ASTM E384-2010 [65] was used to obtain consistent hardness results. Indentations were spaced at a distance of at least four times the diagonal of the previous indent as per ASTM C1327-2008 to avoid strain-hardening effects and possible cracking of the WC particles [66].

A micro-Vickers hardness indenter (Tukon 2500, Wilson Hardness, Norwood, MA, USA) was used to measure if there was a localized improvement in the hardness near carbides due to the high velocity impact of the harder carbide particles into the nickel matrix of the WC-Ni MMC coating. A total of twenty (n = 20) indentations were conducted on a 50WC-50Ni coating. Ten indents were conducted in the matrix, but approximately 5 μm away from the carbide. The indents were taken below the carbide because that was where the impact occurred. Also ten indents were conducted in the matrix, where no carbides were nearby. Each indentation was formed by a 10 gf load for a dwell time of 10 s. This force was used to minimize any effects of the WC-based particles that could be underneath the exposed surface. The same procedures were followed as the hardness procedure mentioned above to avoid strain hardening effects and possible cracking of the reinforcing WC-based particles.

2.5 X-ray Diffraction

X-ray diffraction (XRD, Geigerflex or Ultimate IV, Rigaku, Sendagaya, Japan) was used to determine if decarburization of WC in the final coating had occurred. A cobalt and copper anode was used to characterize the powder and cold-sprayed coatings, respectively. The cobalt anode was used at 40 kV and 30 mA and a graphite monochromator was used to filter K-beta wavelengths. The copper anode was used at 40 kV and 110 mA with a curved graphite monochromator. Continuous XRD mode, where the 2θ diffraction angle was changed from 20° to 120° at a rate of 3° per minute, was used.

2.6 Deposition Efficiency

The deposition efficiency was determined for the WC-Ni mechanical powder blends. The masses of the original grit blasted substrates and coated substrates were measured using a precise balance scale (682B, Mettler Instrumente AG, Zurich, Switzerland). The original mass and the final mass of the mechanical blends were measured using a balance scale (Scout Pro SP2001, McMaster-Carr, Cleveland, OH, USA). The deposition efficiency was calculated using the following equation:

$$DE = \frac{m_{CS} - m_S}{m_{OPB} - m_{FPB}} \times 100\%, \quad (2)$$

where DE is the deposition efficiency and m is the mass (g). The subscripts CS, S, OPB, and FPB represent coated substrate, substrate, original mass of powder blend, and final mass of powder blend, respectively. The deposition efficiency was measured two times for each powder/coating system.

2.7 Dry Abrasion Testing

Dry abrasion testing was conducted on the WC-Ni MMC coatings that were deposited onto low carbon steel substrates according to ASTM G65-2004 [67]. Procedure B – 2000 revolutions was selected for the coatings that contained 66 wt.% WC coating content, Procedure E – 1000 revolutions for the remainder of the WC-Ni MMC coatings, and a modified Procedure E – 100 revolutions for the nickel control coatings [67]. These decisions were made to ensure that the abrasive media did not wear away the coating to expose the underlying substrate. Two samples (n = 2) were tested for each coating composition. Due to the unavailability of chlorobutyl rubber, as required by the ASTM standard, a neoprene compound was substituted to line the test wheel. The hardness of the neoprene was approximately 60 shore A Durometer, which is the same hardness as that suggested by the standard. The rotational speed of the wheel was 200 RPM and a load of 130 N was applied to the specimen. The resulting sliding distance for Procedures B and E was 1436 m and 718 m, respectively. The sliding distance for the shorter test on the cold-sprayed nickel coating was 72 m. AFS 50/70 silica (US Silica, Ottawa, IL, USA) was used as the abrasive media (see Fig. 8), as per the suggestion of the ASTM G65-2004 standard [67]. The abrasive media was

added into a hopper that allowed the sand to flow at a rate of 365 g/min. Figure 9 shows the experimental assembly for the ASTM G65-2004 test [67] and how the abrasive is fed in between the wheel and the coated substrate. To determine the weight loss of the WC-based MMC coatings, the specimens were weighed before and after the test. The volume loss was determined, as suggested by ASTM standard G65-2004, and the wear rate (W), in mm^3/Nm, was determined by dividing the volume loss (Δv), in mm^3, by the applied load (P), in Newtons, and the sliding distance (s), in m, as shown in Eq. (3):

$$W = \frac{\Delta v}{P * s}. \tag{3}$$

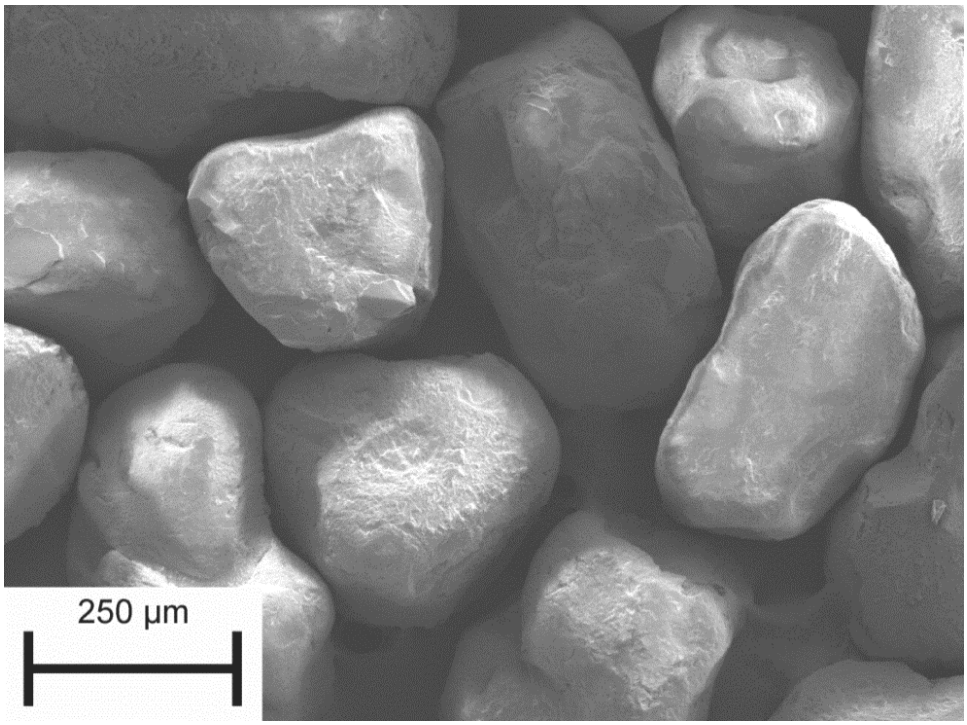

Figure 8: Morphology of AFS 50/70 silica sand

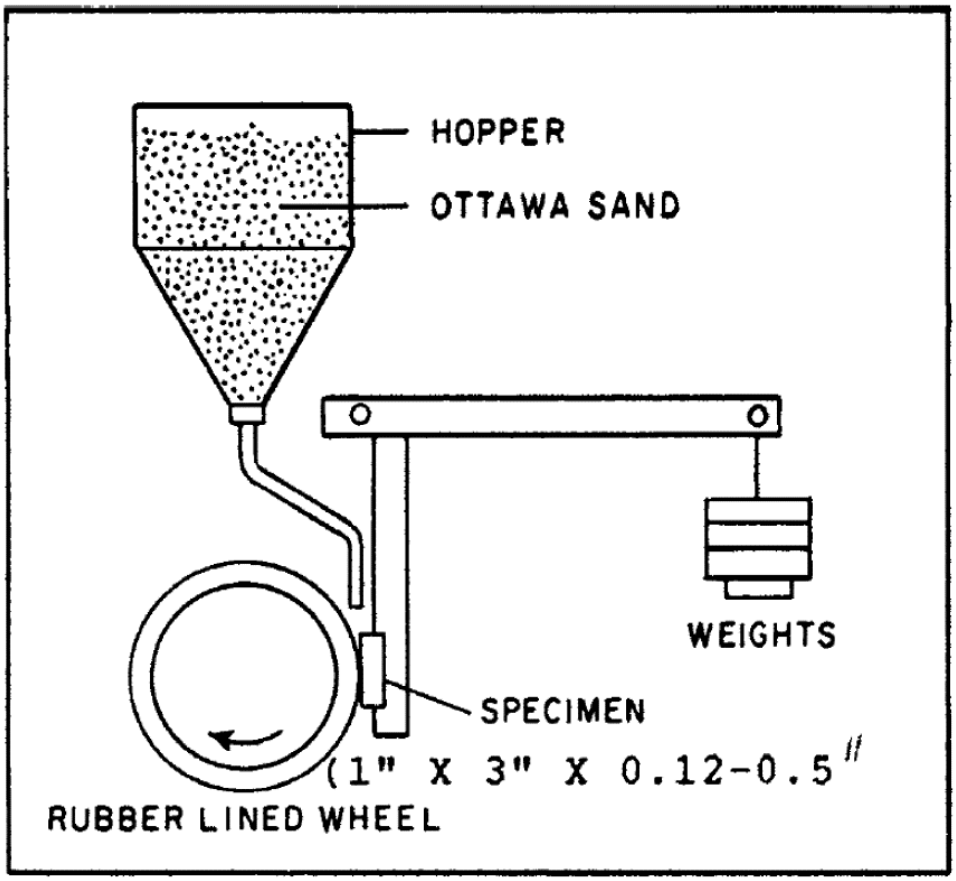

Figure 9: Schematic of ASTM G65-2004 dry abrasion test [67]

3. Results and Discussion

The present study has focused on the development of WC-based MMC coatings through the use of a low-cost, low-pressure cold spray system. Three different mechanical blends were explored in this study, where a WC-based powder was mixed with copper and nickel powders or with nickel powder to fabricate MMC coatings. The following sections will discuss the results of the tests conducted on the various MMC coatings.

3.1 WC-Ni-Cu

3.1.1 Purpose

The purpose of this study was to fabricate WC-based MMC coatings with improved hardness, and to take advantage of solution strengthening of the Ni-Cu matrix. Also, the addition of Cu in the mechanical blend allows coating deposition at lower working fluid temperatures because it is a softer metal, in comparison to nickel. Furthermore, it was important to understand how the parameters of the cold spray system and the mechanical blend composition affect the fabricated coating microstructure (WC coating content) and hardness. Finally, it was necessary to determine if decarburization or oxidation would occur because that would likely reduce the mechanical integrity of the MMC coatings.

3.1.2 Variation of Parameters

Variation of the cold spray parameters for fabrication of the MMC coating was crucial because it affects the microstructure of the coating, which ultimately has an impact on mechanical properties. In order for a set of parameters to be considered optimized the coating must have i) a thickness of at least 300 μm, ii) a high WC content with uniform homogeneous distribution through the coating, and iii) a high hardness, which was determined by comparing the different fabricated coatings. The parameters that can be modified for the cold spray unit itself are the temperature and the pressure of the working fluid (compressed air). The parameters that can be modified that involve the interaction between the torch and the substrate are the stand-off distance (distance between the substrate and the torch), the traverse nozzle velocity, the number of passes, and the increment at which the torch moves up across the substrate. Finally, the rate at which the powder is fed into the torch can be modified. The microstructures of each fabricated coating will be examined in the following sub-section.

3.1.3 Microstructural Analysis

It was important to determine the WC content in the fabricated MMC coatings because an increased presence of hard reinforcing WC particles should improve the hardness of the coatings. SEM images provide qualitative confirmation of the content of the WC reinforcing particles in the coatings. Figure 10 shows a coating that was fabricated from a 35 wt.% WC + 30 wt.% Ni + 35 wt.% Cu mechanical powder blend, where three microstructural features were easily distinguishable.

EDS analysis determined that the bright phase was WC because the area was rich in tungsten. Carbon was not quantified because the coatings were carbon coated, making it difficult to determine the carbon content. The darker phase was the Ni-Cu matrix. Since nickel and copper have a similar atomic number, 28 and 29 respectively, it was difficult to distinguish between the two phases using SEM and ImagePro. However, that will not affect image analysis and the determination of coating density because nickel and copper have very similar densities, 8900 kg/m^3 and 8930 kg/m^3, respectively [68]. The black areas were determined to be pores because a large amount of carbon was present in those areas. The presence of carbon may be due to carbon coating or the presence of resin that filled the void. Also, the presence of depth in SE images, as seen in Fig. 11, suggests that those areas were pores.

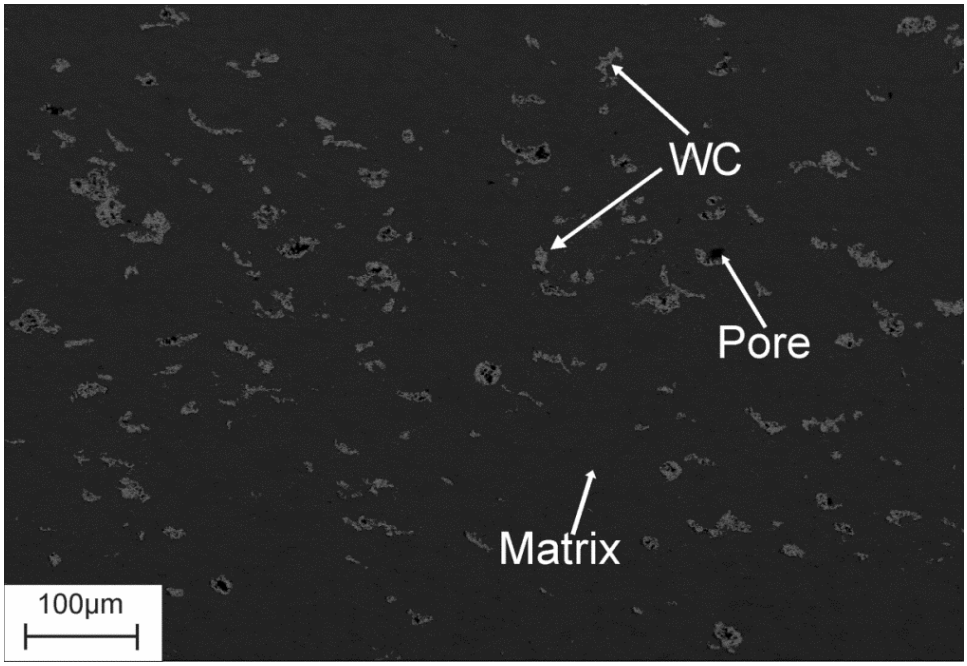

Figure 10: Coating microstructure of 35WC-30Ni-35Cu showing three different phases

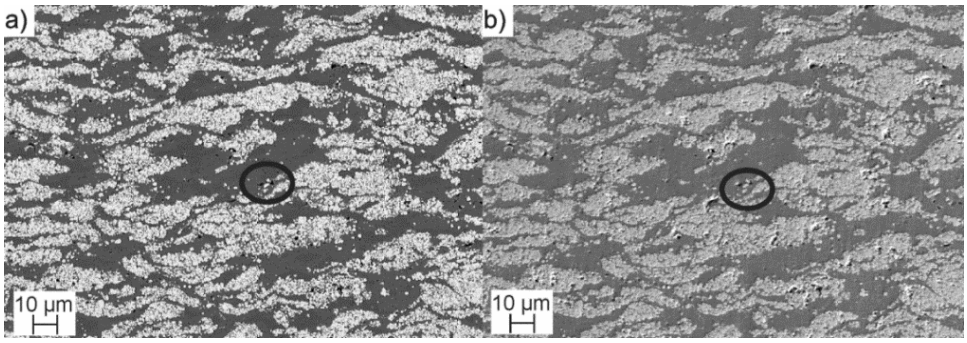

Figure 11: Magnified image of 96WC-2Ni-2Cu showing pores: *a*) BSE and *b*) SE mode

It was necessary to determine the weight % (wt.%) of the WC particles in the coating to approximate how much of the particles from the mechanical powder blend were deposited into the MMC coating. This will provide quantitative information on the WC deposition efficiency. An approximate density of each MMC coating was calculated using parallel path averaging, as shown in Eq. 4, to

convert the WC content from vol.% to wt.%. The density of WC was assumed to be 15,800 kg/m^3 [68] because the binder content in the WC-based feedstock powders was low (12 wt.%). When the binder was neglected, there was a density difference of 9% when compared to the parallel path averaging density of bulk WC-10Ni-2Cu. Therefore, the presence of the binder in the coating was ignored as it did not have a significant effect on the overall coating density. It was difficult to differentiate between the copper and nickel phases in the SEM micrographs because they had very similar brightness intensities in BSE mode. However, they have very similar densities and can be assumed to be one phase. With the ImagePro software, it was determined that the porosity of the cold-sprayed coatings was low (less than 7.4 vol.% in all cases). Given the low porosity values, the pores were assumed to be negligible when converting vol.% of WC to wt.%. Further, the density of gas that may have filled the pores is much lower than that of the WC-based particles and the metal matrix.

$$\rho_{\text{composite}} = (\text{vol.\% WC})\rho_{\text{WC}} + (\text{vol.\% Ni/Cu})\rho_{\text{Ni/Cu}} \quad (4)$$

There are a variety of parameters that can be varied for the cold spray unit. The temperature and pressure of the working fluid were kept constant at 475ºC and 88 psig because thick adherent coatings were fabricated using these parameters. Furthermore, these parameters were guidelines suggested by SST Centerline Ltd. to fabricate coatings using their copper powder. These parameters were followed closely because copper oxidizes easier than nickel. Any oxidation of copper

would be detrimental to the ductility of the overall coating, negatively affecting the mechanical properties of the MMC coating.

Two types of powder feeders were examined in this study, a gravimetric powder feeder that was built into the cold spray unit and a volumetric powder feeder that was separate from the cold spray unit. Figure 12 shows the gravimetric powder feeder, while Fig. 13 shows the volumetric powder feeder set-up. The gravimetric powder feeder controls the rate at which the powder is fed into the torch by a valve that is controlled by the operator on the touch screen. The feed rate is expressed as a percentage of the maximum mass flow rate. The volumetric powder feeder controls the rate at which the powder is fed into the torch by adjusting the pressure and volumetric flow rate of the carrier gas (argon). Those parameters control the minimum flow meter reading (FMR); however, the FMR can be further increased if necessary.

Figure 12: *a)* Cold spray control unit and *b)* zoomed image of gravimetric powder feeder in cold spray control unit

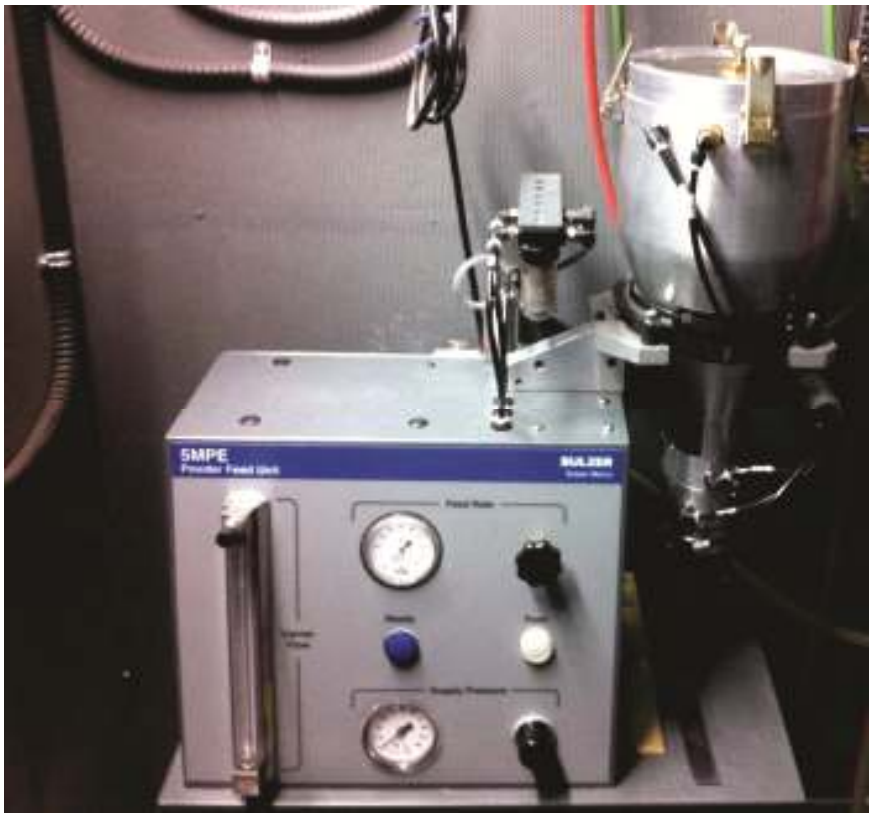

Figure 13: Image of Sulzer-Metco 5MPE volumetric powder feeder

The microstructures of the coatings fabricated by a 35WC-30Ni-35Cu mechanical blend, using either the gravimetric powder feeder or the volumetric powder feeder were examined, while keeping the remainder of the parameters constant. Figure 14 shows that more WC reinforcing particles are present in the deposited MMC coating when the powder blend is fed by the volumetric powder feeder. The WC content of the coatings were 3.9 ± 0.3 vol.% (n = 3) and 4.9 ± 0.6 vol.% (n = 3) for those fabricated by the gravimetric powder feeder and volumetric powder feeder, respectively. It is very likely that the coatings fabricated using the volumetric powder feeder contained a higher WC content because of an increase in particle velocity due to the addition of pressurized argon, increasing adhesion to the metal matrix. Therefore, from these results, it was determined that the powder should be transported to the cold spray unit using the volumetric powder feeder to fabricate WC-based MMC coatings because it should show improved properties.

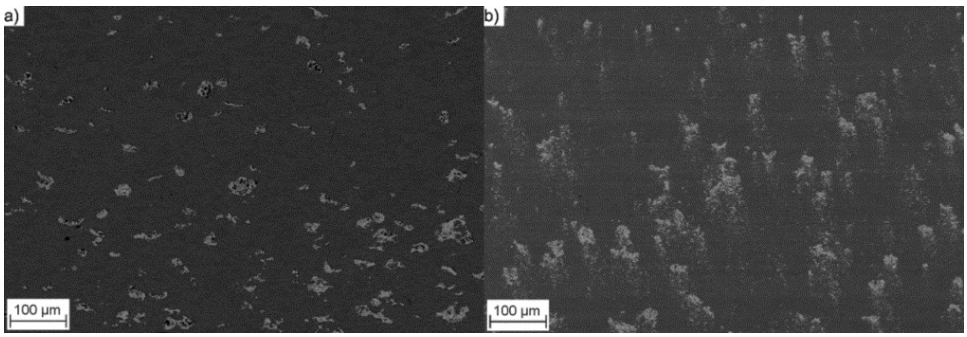

Figure 14: Microstructure of coating fabricated with a 35WC-30Ni-35Cu mechanical blend using: a) the gravimetric powder feeder and b) the volumetric powder feeder

Studies have shown that as the stand-off distance and the traverse nozzle velocity decreases, there is improved heating of the substrate [24, 69]. Therefore, various stand-off distances and traverse nozzle velocities were explored when depositing a 92WC-6Ni-2Cu mechanical blend. Table 4 shows the effect of the variation of nozzle passes, nozzle velocity, and stand-off distance on WC content in the coating and the WC deposition efficiency. The trends from Table 4 show that the highest WC content was achieved by the 92WC-M-5 coating; however, its thickness did not meet the requirements of being at least 300 μm, and was 142 μm. Studies have shown that when cold spraying harder materials, the coating may begin to erode away, making it difficult to achieve an appropriate coating thickness with an increased number of passes [15, 16]. Table 4 also shows that as the stand-off distance increases, the WC content in the coating decreases significantly. These results suggest that stand-off distance has a greater effect on WC deposition efficiency and that a 5 mm stand-off distance yielded the desired final coating because it improved the heating effects onto the substrate. Therefore, the optimized parameters were the parameters used to deposit the 92WC-S-5 coating because it required the least amount of passes to obtain at least a 300 μm thick coating and that had a good WC deposition efficiency.

Table 4: Parameters used to understand the effects of traverse nozzle velocity and stand-off distance

Sample	**Passes**	**Nozzle velocity (mm/s)**	**S.O.D. (mm)**	**WC content in coating (vol.%) (*n* = 3)**	**WC content in coating (wt.%) (*n* = 3)**	**WC deposition efficiency (*n* = 3)**
92WC-S-5	2	5	5	35.3 ± 0.8	49.2 ± 0.9	53.4 ± 1.0
92WC-M-5	2	7	5	49.2 ± 4.2	63.1 ± 3.8	68.6 ± 4.2
92WC-F-5	4	15	5	43.1 ± 2.2	57.3 ± 2.2	62.3 ± 2.4
92WC-F-7.5	4	15	7.5	34.8 ± 0.7	48.7 ± 0.8	52.9 ± 0.9
92WC-F-10	4	15	10	30.6 ± 1.4	43.9 ± 1.7	47.7 ± 1.8

Figure 15 shows the effects of traverse nozzle velocity on the microstructure of the coating, while Fig. 16 shows the effects of stand-off distance on the microstructure of the coating. As mentioned previously, the 92WC-S-5 coating was the only one thick enough that was fabricated using two passes. Both figures exhibit a non-homogenous structure because there were regions with a high content of WC and a high content of matrix.

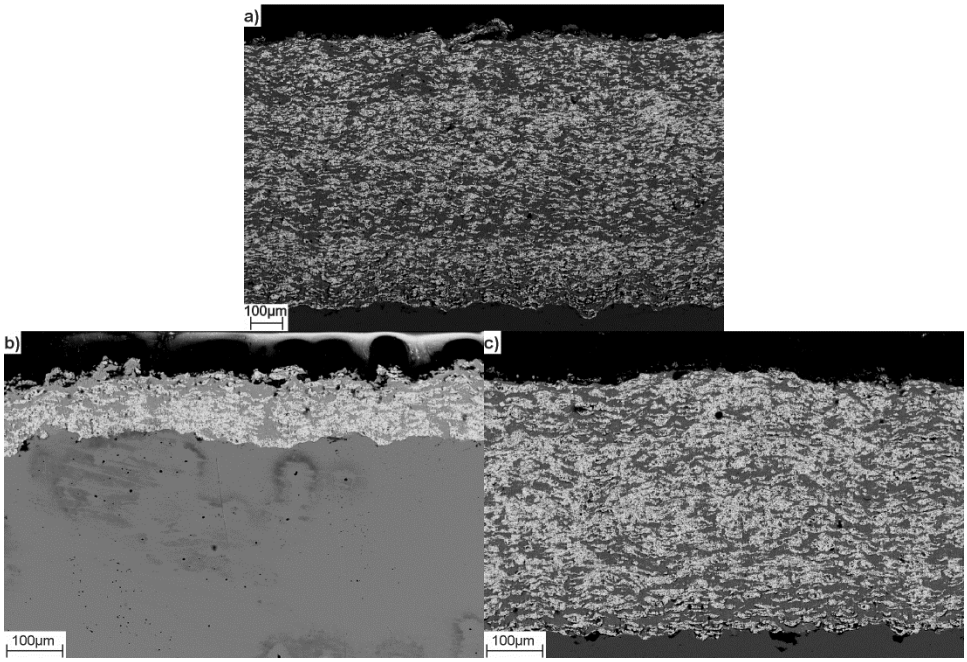

Figure 15: SEM micrographs of coatings fabricated using a 92WC-6Ni-2Cu mechanical blend using various traverse nozzle velocities: *a*) 5 mm/s, *b*) 10 mm/s, and *c*) 15 mm/s

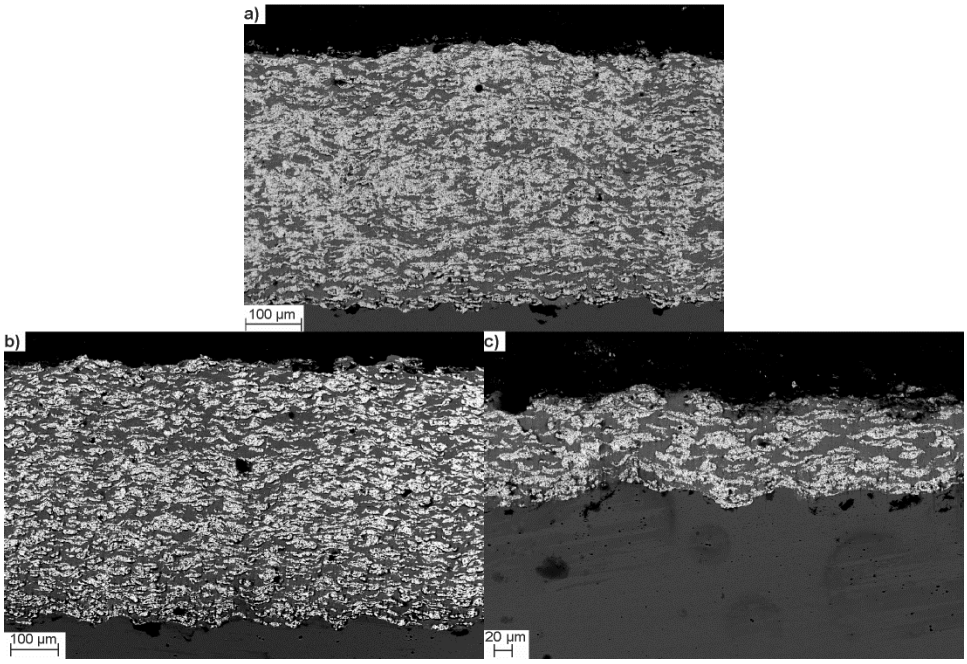

Figure 16: SEM micrographs of coatings fabricated using a 92WC-6Ni-2Cu mechanical blend using various stand-off distances: *a*) 5 mm, *b*) 7.5 mm, and *c*) 10 mm

After varying the parameters, it was important to understand the effects of powder blend composition on the final coating composition because there may be a point where more WC-10Ni-2Cu particles in the mechanical blend will lower the amount of WC reinforcing particles in the fabricated MMC coating.

Various powder blends were explored to determine which composition produced coatings with the highest WC coating content. Figure 17 shows the relationship between the WC content in the coating (in vol.% or wt.%) and the WC content in the powder blend (in wt.%). The figure shows that there was a direct relationship between the WC content in the coating and that in the powder blend. The coating that was produced from the 96WC-2Ni-2Cu powder blend produced the optimal coating in terms of WC content in the coating, with a WC deposition efficiency of 57 ± 0.8%. Table 5 shows the WC deposition efficiency of each coating fabricated using the various mechanical blend compositions. The 96WC-2Ni-2Cu powder blend produced a coating that contained 54 ± 0.8 wt.% WC (n = 3).

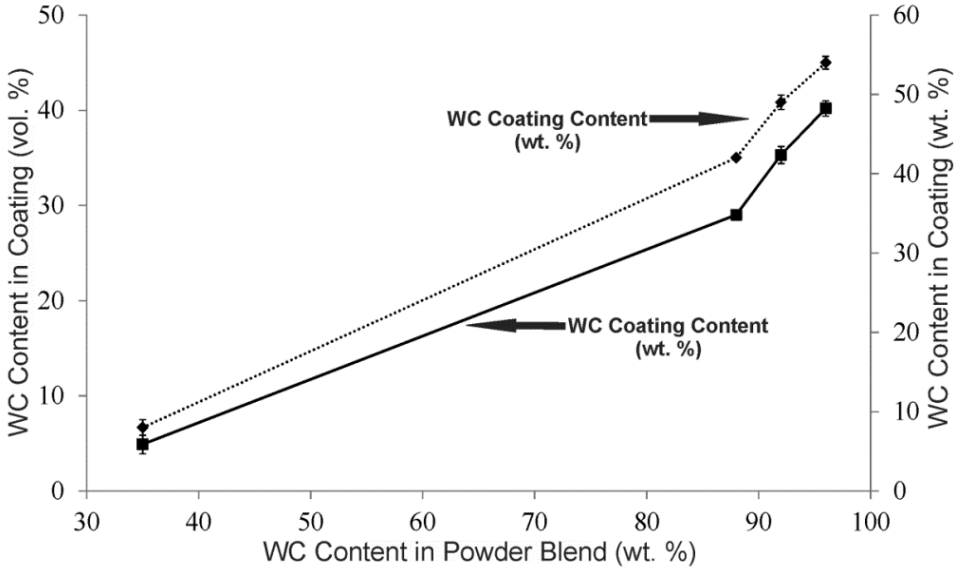

Figure 17: Relationship between the WC content in the coating and the WC content in the mechanical powder blend

Table 5: WC content in coating and the WC deposition efficiency

Powder blend	**WC content in blend (wt.%)**	**WC content in coating (wt.%) (*n* = 3)**	**Porosity (vol.%) (*n* = 3)**	**WC DE (%) (*n* = 3)**
35WC-30Ni-35Cu	35	9 ± 1.0	0.08 ± 0.06	24 ± 3.0
88WC-10Ni-2Cu	88	42 ± 0.3	2.0 ± 2.0	48 ± 0.4
92WC-6Ni-2Cu	92	49 ± 0.9	2.8 ± 0.3	53 ± 1.0
96WC-2Ni-2Cu	96	54 ± 0.8	0.5 ± 0.1	57 ± 0.8

The impact of the harder, high-velocity WC particles provided reinforcement to the coating. Figure 18 shows that the impact of the particles causes the porous spray-dried agglomerated WC particles to spread out. Figure 19 shows the microstructure of the pure Cu, while Fig. 20 shows the microstructure of the pure Ni coating. The pure Cu coating adhered well to the substrate and had a porosity of approximately 2.8 ± 1.1 vol.% (n = 3). The coating was homogeneous because there were no localized areas with a high or low amount of porosity, unlike the cold-sprayed pure Ni coating (see Fig. 20). This is likely due to the softer nature

of copper because the splats were often flattened rather than round-like. The porosity of the pure Ni coating was approximately 10.7 ± 8.9 vol.% (n = 3). The standard deviation of the cold-sprayed Ni coating was high because there were three areas with different porosities. The porosity of each individual area was analyzed at a higher magnification in attempt to capture the localized porosity. The porosity of the nickel coating closest to the substrate was the highest at 17.2 ± 0.5 vol.%. The high porosity could be due to poor interaction between the impacting particles and the substrate, suggesting that it was very difficult to deposit pure nickel using these parameters. The porosity of the mid-section and top-section of the pure nickel coatings had a porosity of 1.0 ± 0.4 vol.% and 13.4 ± 2.9 vol.%, respectively. This trend of having porous regions near the surface of the coating has been observed when fabricating titanium coatings using cold spraying [70]. It was difficult to deposit nickel using these parameters; however, with the addition of the softer copper, nickel can be added to enhance the hardness of the coating. Furthermore, Table 5 shows that the porosities of the WC-Ni-Cu coatings were typically lower than the porosities of the pure copper and nickel coatings. This suggests that the impact of the WC particles likely improved the density of the WC-Ni-Cu MMC coatings.

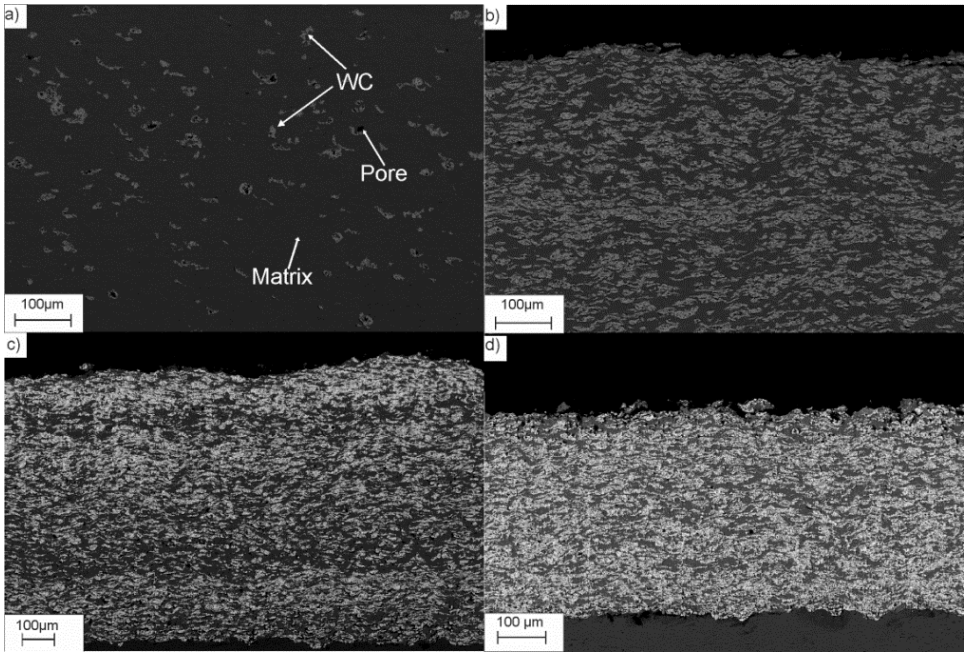

Figure 18: Microstructure of coatings that were fabricated using a *a*) 35WC-30Ni-35Cu, *b*) 88WC-10Ni-2Cu, *c*) 92WC-6Ni-2Cu, and *d*) 96WC-2Ni-2Cu mechanical blend

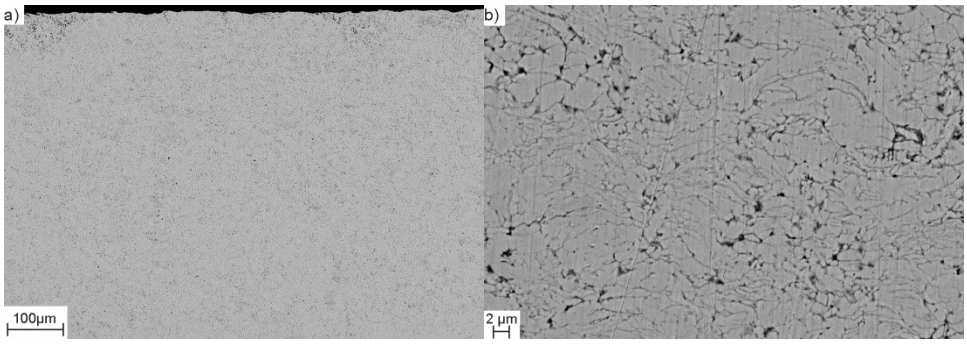

Figure 19: Microstructure of pure cold-sprayed copper *a*) overview and *b*) magnified image

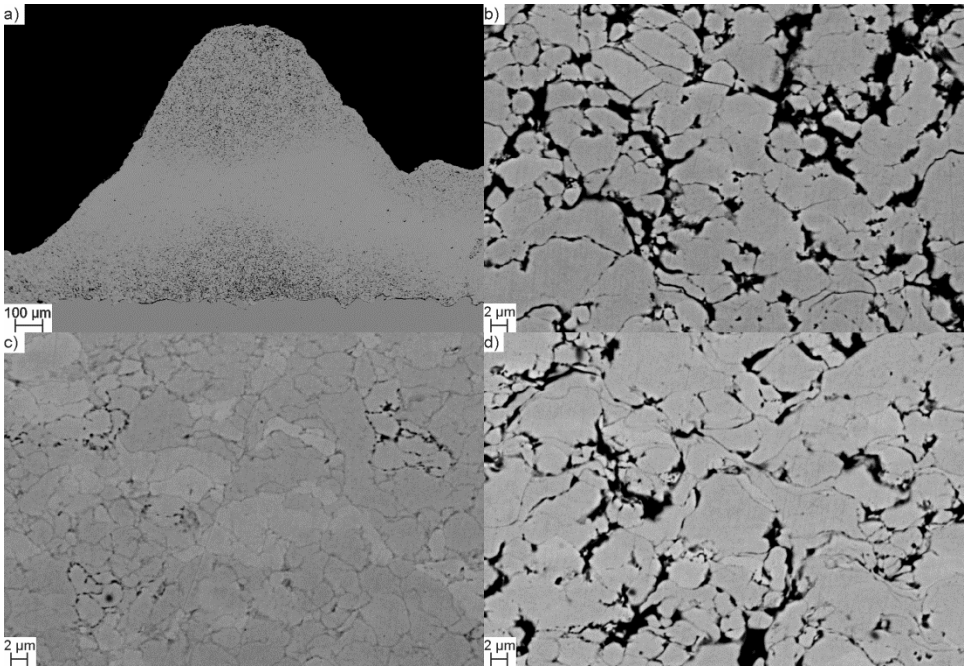

Figure 20: Microstructure of pure cold-sprayed nickel *a*) overview, *b*) near coating/substrate interface, *c*) middle/dense region, and *d*) top/porous region

3.1.4 Vickers Micro-hardness

Hardness indentations were conducted to determine which parameters and powder blend produced a MMC coating with enhanced properties. Ultimately, the coating with the highest hardness would be deemed to have superior wear resistance. However, hardness is not the sole indicator of how a coating will perform under abrasive conditions, but it stands as a good indicator.

First, the hardness of the coatings fabricated using either the gravimetric or volumetric powder feeder were tested. Although the coatings fabricated using the volumetric powder feeder produced coatings with a higher WC content in the coating, there was no significant difference in coating hardness. The hardness of the coatings fabricated using the gravimetric and volumetric powder feeder were

171 ± 15 $HV_{0.3}$ (n = 50) and 169 ± 11 $HV_{0.3}$ (n = 50), respectively. The small increase in WC content did not have a significant effect on the hardness of the coating. The volumetric powder feeder was chosen as the method to feed the powder to the cold spray torch because of the higher coating WC content that was produced in the coating.

The effects of stand-off distance and nozzle velocity on the coating hardness were examined because those parameters have shown to increase the temperature of the substrate surface. Table 6 shows the hardness of the coatings that were fabricated using various stand-off distances and nozzle velocities. Samples 92WC-S-5 and 92WC-F-7.5 had the highest hardness of approximately 355 $HV_{0.3}$. It is reasonable that both of these coatings yielded similar hardness values because they had very similar WC coating content, as seen in Table 4. Furthermore, Table 4 shows that 92WC-M-5 had the highest WC coating content; however, it produced the lowest hardness of all the coatings investigated when varying stand-off distance and traverse nozzle velocity. This could be due to the non-homogeneity of the distribution of the WC particles in the coating. This coating also had the highest standard deviation of WC content (see Table 4). It is possible that the coating did not have the same composition below the exposed surface. If there were less WC particles below the exposed surface, there would be less load sharing between the WC particles, which would result in a lower coating hardness. Finally, after four passes, sample 92WC-F-10 was not thick enough to conduct hardness indentations. Since the fewest amount of passes to fabricate a coating is desired, sample 92WC-F-10 was not explored further.

Table 6: Hardness of fabricated coatings sprayed at different stand-off distances and nozzle velocities

Sample	Hardness ($HV_{0.3}$) (n = 50)
92WC-S-5	355 ± 61
92WC-M-5	283 ± 29
92WC-F-5	308 ± 30
92WC-F-7.5	355 ± 71
92WC-F-10	Not thick enough

After determining that a stand-off distance of 5 mm and a traverse velocity of 5 mm/s was optimal for this system, the composition of the mechanical blends was varied because a higher amount of WC was deposited into coatings that had a higher WC content in the mechanical blend. Figure 21 shows the relationship between the WC coating content and the hardness of the coating. A linear trend between WC coating content and hardness was observed. The highest hardness was achieved by the coating fabricated using the 96WC-2Ni-2Cu powder blend. The hardness of the coating was 385 ± 73 $HV_{0.3}$ (n = 50).

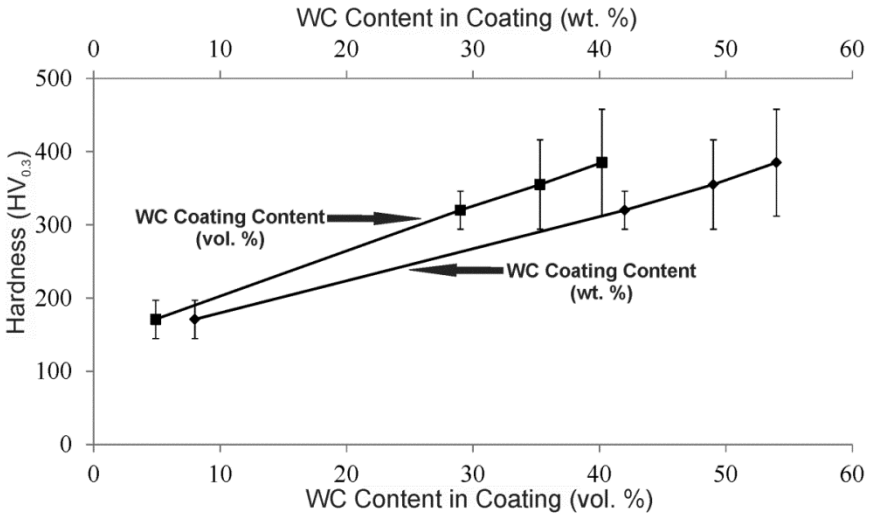

Figure 21: Curve of Vickers micro-hardness versus WC content in the coating

In order to understand further the effects of the reinforcing particles on the hardness of the matrix, pure copper and pure nickel coatings were fabricated. The hardness of the pure copper coating and the pure nickel coating was 103 ± 20 $HV_{0.3}$ and 136 ± 18 $HV_{0.3}$, respectively. The coatings had hardness values that were higher than their bulk hardness values but close to their cold-worked hardness values [71]. The reported hardness values of cold-worked copper and cold-worked nickel are approximately 95 HB and 151 HB, which is approximately 95 HV and 151 HV, according to ASTM standard E140-2007 [72]. The improved hardness could be due to work hardening, adiabatic shear instability, and dynamic recrystallization. These mechanisms have been observed in both high and low-pressure cold-sprayed coatings [12, 73, 74].

The hardness of the fabricated WC-Ni-Cu MMC coatings containing the highest WC coating content (~400 HV) were much lower than those typically seen in WC-Co coatings fabricated using HVOF spraying (~800–1400 HV) [29 - 34]. However, the addition of the WC-based particles improved the hardness of the MMC coating because it increased the hard phase content and yielded coatings with lower porosity than those observed in the monolithic metallic coatings.

Wang and Villafuerte [21] have studied WC-based MMC coatings that were fabricated from WC particles that were coated with 20 wt.% Cu (80 wt.% WC content). A cold-spraying system operating at low pressure was used. In their study, it was found that the hardness of the coating was approximately 200 HB. The ASTM Standard E140-2007 [72] suggests that a hardness of 200 HB is

approximately equal to 200 HV, using the Brinell to Vickers hardness conversion charts for metals. In this study, a hardness value which was nearly double that measured by Wang and Villafuerte [21] was found. The coatings in this study were fabricated by mechanically blending WC with nickel and copper powders. It was found that the WC content of the cold-sprayed coating was not equal to the WC content in the mechanically blended powder, as was the case with the coatings fabricated using copper coated WC powder. The mechanically blended powder, after spraying, contained less WC than the original powder blend, suggesting that the addition of nickel in the matrix enhanced the hardness, in part, of the MMC coating.

3.1.5 X-ray Diffraction (XRD)

Decarburization of the WC phase of thermal-sprayed coatings reduces the mechanical integrity of the coating system [31]. XRD was used to determine which materials and phases were present in the feedstock powder and the fabricated MMC coatings. Each cold-sprayed MMC coating fabricated in this study displayed no decarburization or oxidation. Therefore, only the XRD profiles of the coatings fabricated using various mechanical powder blends at the optimized parameters were presented. Figure 22 shows the XRD profile of the WC-based powder and Fig. 23 shows the XRD profiles of each coating fabricated using various powder mechanical blends with the optimized parameters. W and W_2C were not present in any of the as-sprayed coatings, confirming that decarburization did not occur. Also, no oxides or amorphous phases were present in any of the cold-sprayed MMC coatings, maintaining the ductile metal matrix

phase. Furthermore, the XRD profiles of each as-sprayed coating were very similar to the WC-10Ni-2Cu feedstock powder, which additionally supports that no chemical changes occurred.

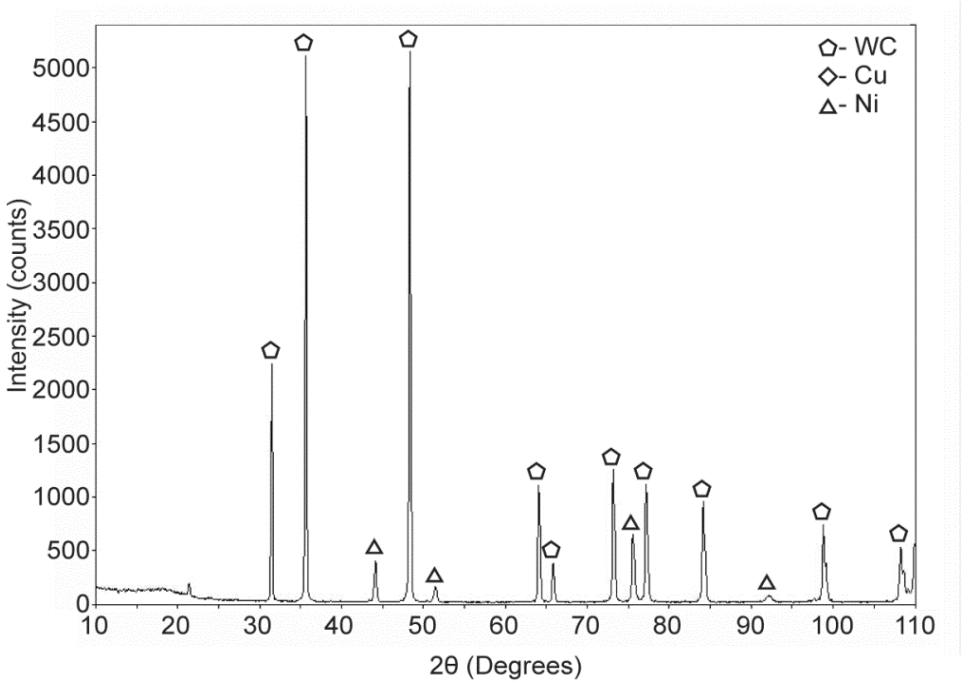

Figure 22: XRD profile of the nano-agglomerated WC-10Ni-2Cu powder

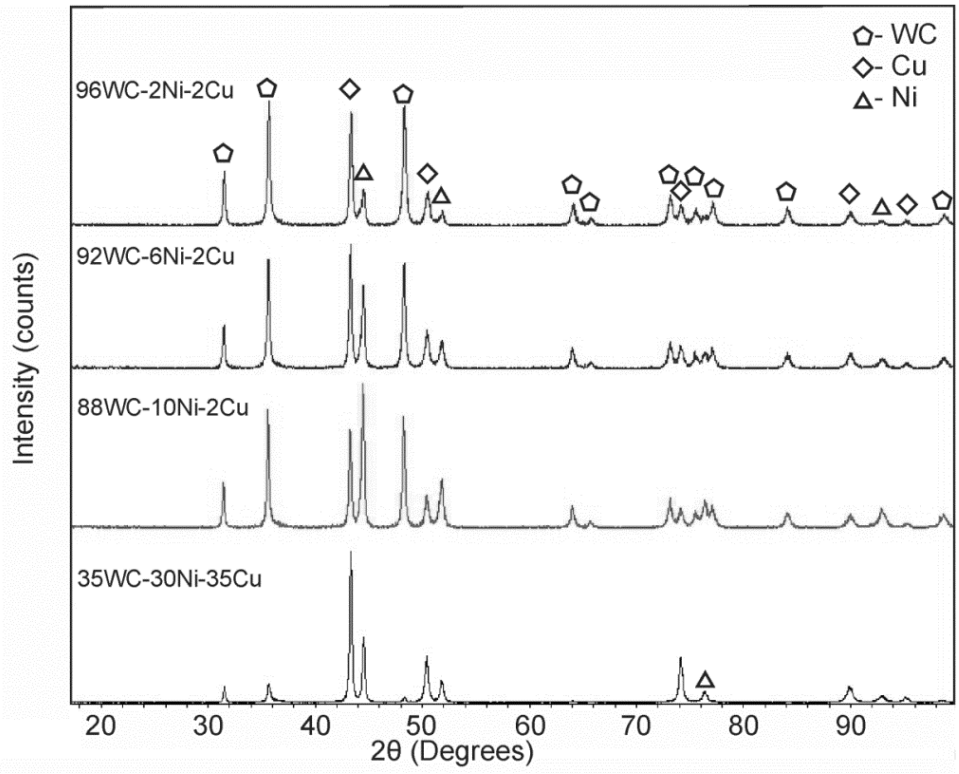

Figure 23: XRD profiles of the various compositions used to fabricate WC-Ni-Cu coatings under optimized parameters

Figure 23 shows that as the WC content in the powder blend increases, the maximum intensity peak in the fabricated coating for WC ($2\theta = 48°$) increases relative to the copper ($2\theta = 43°$) and nickel ($2\theta = 44°$) maximum intensity peaks, which is in agreement with the SEM micrographs of Fig. 18. However, the copper (and occasionally the nickel) peaks were also large, suggesting there was a significant amount of the ductile phase present. The 96WC-2Ni-2Cu powder blend produced the optimum combination of WC and ductile phases in the final coatings because the intensities of the ductile phases decreased significantly when compared to the coatings fabricated from the other powder blend compositions.

Figures 24 and 25 show the XRD profiles of cold-sprayed copper and nickel coatings, respectively. It should be noted that XRD was conducted on the nickel

coating that was cold-sprayed at 550°C. If no oxidation was detected after deposition at a temperature of 550°C, then no oxidation should be observed at a deposition temperature of 475°C. Figure 24 shows that the cold-sprayed copper coating was partially oxidized. However, the Cu_2O content was very low; it may have contributed to increasing the overall hardness of the pure copper coating as mentioned in Section 3.1.4. None of the MMC coatings fabricated using the optimized parameters had detectable oxide levels in the XRD profiles or significant levels of oxygen in EDS mapping. This could be due to the impact of the hard WC-Ni-Cu agglomerated particles when they impact the coating and erode any oxide layer from the deposited coating.

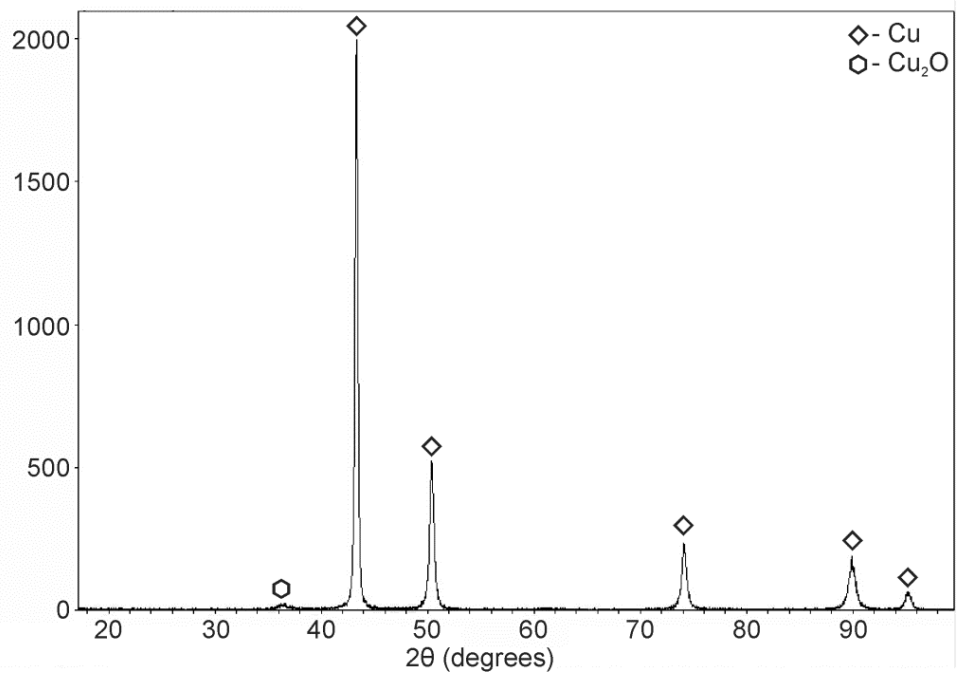

Figure 24: XRD profile of cold-sprayed copper coating at 475°C

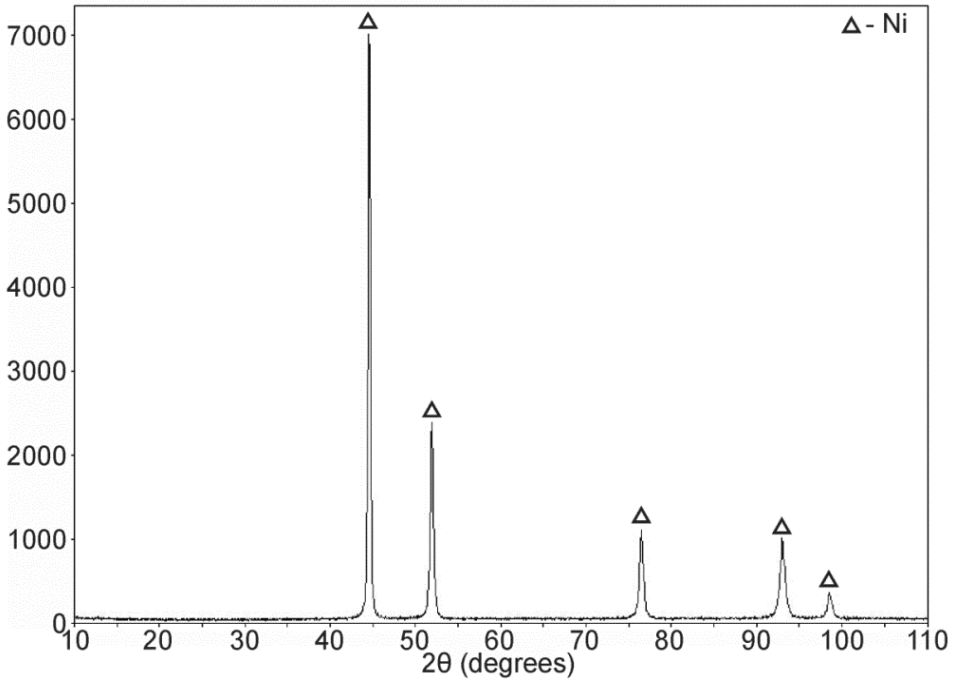

Figure 25: XRD profile of cold-sprayed nickel coating at 550°C

3.1.6 Concluding Remarks

Typically, WC-12Co coatings that are fabricated by HVOF spraying have a hardness of 800–1400 HV [29 - 34], which is significantly higher than that of the coatings examined in this section. In an attempt to fabricate coatings with higher hardness values, copper will be removed.

3.2 WC-Ni MMC Coating

3.2.1 Purpose

The purpose of this section was to examine the feasibility of depositing WC-based particles with nickel to fabricate WC-Ni MMC coatings. Copper was removed because there was too much copper in the fabricated WC-Ni-Cu MMC coatings, which resulted in soft coatings. Nickel was explored as the sole binder because it is harder than copper and has superior corrosion resistance. Coating characterization was conducted on the various MMC coatings to determine how the WC content in the mechanical powder blend affected the WC content in the coating, the coating porosity, hardness and wear resistance. XRD was also used to confirm that no chemical changes occurred after deposition. Additionally, it was crucial to determine if the wear rate of the coating was linearly related to the coating hardness because that would provide a method to approximate the wear rate without conducting costly and time consuming wear tests.

3.2.2 Variation of Parameters

Due to the extensive coating characterization completed in Sections 3.1.3 and 3.1.4, the parameters used for deposition of the WC-Ni MMC coatings were nearly the same as those used to deposit the WC-Ni-Cu MMC coatings. However, due to the harder nature of nickel, a higher temperature and higher pressure was required to fabricate a coating that adhered well to the substrate. The only temperature and pressure that permitted successful deposition of a coating was

550°C and 92 psig. It was not possible to achieve higher working fluid temperatures with this cold spray model, prohibiting the exploration of higher temperatures. Higher pressures were examined; however, the coating deposition was very poor and coatings partially spalled off during deposition.

3.2.3 WC Content[1]

This section has focused on the development of a WC-based MMC coating through the use of a low-cost, low-pressure cold spray system. Figure 26 shows the microstructure of the coatings that were fabricated from the different feedstock powder compositions of the WC-based mechanical powder blends. It was clear from the SEM images that there were two distinguishable phases present in the WC-based MMC coatings. EDS analysis determined that the bright phase was WC because the area was rich in tungsten with some cobalt present. Carbon was not quantified because the coatings were carbon coated, making it difficult to determine the carbon content. The darker phase was the nickel matrix. The black areas were determined to be pores because carbon was the main element when EDS was conducted on those areas. The presence of carbon may be due to carbon coating or the presence of resin that filled the void. However, the lack of any other main constituent, like tungsten or nickel, suggests that the black areas were pores. Figure 26 shows that as the WC content increased in the mechanical blends, there was an increase in WC content in the fabricated

[1] Portions of this section were published in: N. Melendez, A. McDonald, "Development of WC-based Metal Matrix Composite Coatings using Low-pressure Cold Gas Dynamic Spraying", *Surf. Coat. Technol.*, 214, 2013, 101 – 109.

coatings. However, the coatings did not show a homogeneous distribution of WC particles in the microstructure because there were some areas of the nickel matrix that were not reinforced by the hard WC particles. This was clearly observed in the coatings that were fabricated from the 75 wt.% WC + 25 wt.% Ni and the 92 wt.% WC + 8 wt.% Ni, where some areas had a high concentration of reinforcing WC particles. A non-homogeneous microstructure was observed in the fabricated coatings because the feedstock powders were mechanically blended and not agglomerated together to form the spray particles.

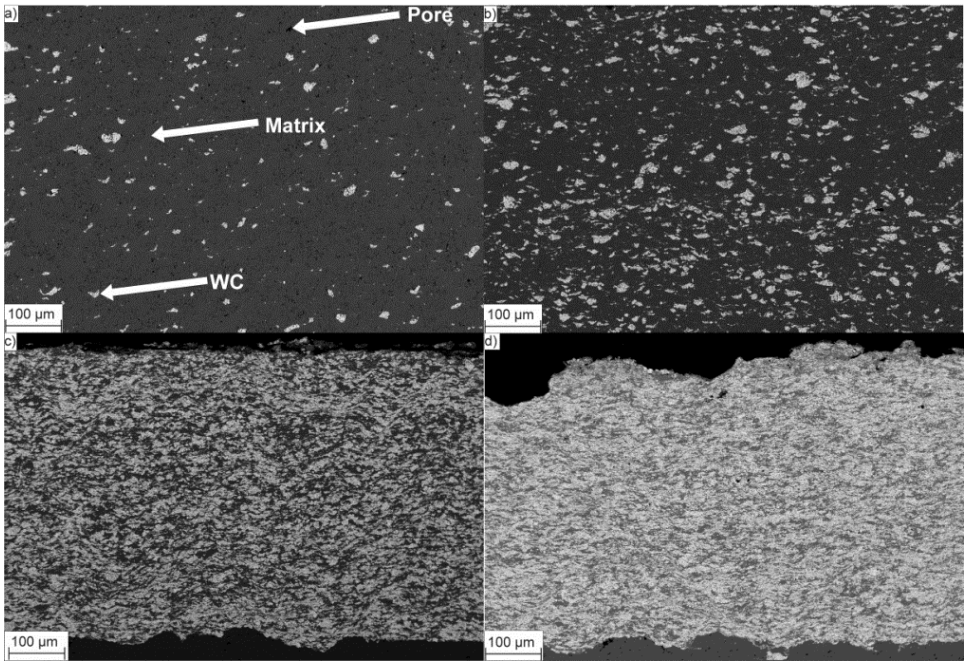

Figure 26: Microstructure of WC-based MMC coatings with feedstock composition of *a*) 50 wt.% + 50 wt.% Ni, *b*) 75 wt.% WC + 25 wt.% Ni, *c*) 92 wt.% WC + 8 wt.% Ni, and *d*) 96 wt.% WC + 4wt.% Ni

It was necessary to determine the weight % (wt.%) of the WC particles in the coating to approximate how much of the particles from the mechanical powder blend were deposited into the MMC coating. This is the WC deposition efficiency. An approximate density of each MMC coating was calculated using

parallel path averaging, as shown in Eq. 5, to convert the WC content from vol.% to wt.%.

$$\rho_{\text{composite}} = (\text{vol.\% WC})\rho_{\text{WC}} + (\text{vol.\% Ni})\rho_{\text{Ni}} . \quad (5)$$

The density of WC was assumed to be 15,800 kg/m^3 [68] since the cobalt binder content in the WC-based feedstock powders was low (12 wt.%). When cobalt was neglected, there was a difference in density of 9% when compared to the parallel path averaging density of bulk WC-12Co. Therefore, the presence of cobalt in the coating was ignored as it did not have a great effect on the overall coating density. The density of nickel was taken to be 8,900 kg/m^3 [68]. The gases trapped in the pores of the coating will contribute to the overall coating density. However, the ImagePro software determined that the porosity of the cold-sprayed coatings was less than 2.2 vol.% for all coatings. Therefore, the entrapped gases in the pores made negligible contribution to the coating density in comparison to WC and nickel, and was neglected.

Figure 27 shows the effect of the WC content in the mechanical blend to the WC content in the coating. This figure shows that as the WC content in the powder blend increased, the WC content in the coating increased. The error bars presented in the graph are one standard deviation. The coatings fabricated by the 92 wt.% WC + 8 wt.% Ni mechanical blend had the highest standard deviation, this was most likely associated with the non-homogeneity of the coatings because there were some localized areas that had a higher WC content, as shown in Fig.

26c. This trend has also been observed in other studies involving low-pressure cold-sprayed aluminum (Al) + alumina (Al_2O_3) MMC coatings [22].

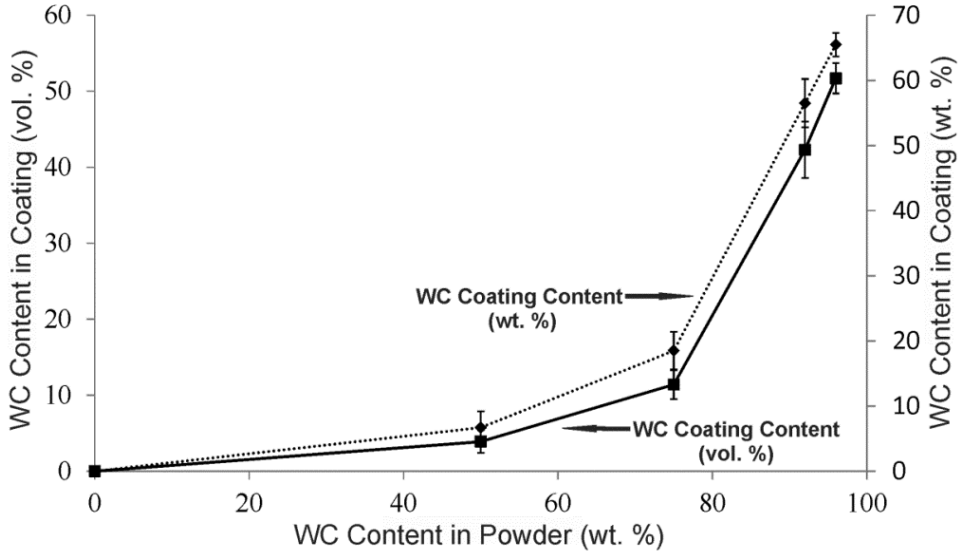

Figure 27: Curve of WC content in the coating versus WC content in the mechanical powder blend

Table 7 presents the coating porosity, the WC deposition efficiency, and the overall deposition efficiency for each mechanical blend, where each value, with the exception of the overall deposition efficiency, is presented as an average along with the standard error of the mean. The standard error of the mean is the standard deviation divided by the square root of the number of measurements, *n* [75]. The standard error of the overall deposition efficiency was not presented because only two measurements were taken; however, the differences between the two measurements were small and never exceeded 0.6%. The number of measurements for each sample is presented in Table 7. As the WC content in the powder blend increased, the deposition efficiency of the WC particles increased. Other studies have shown that when the ceramic content in the feedstock powder

increased, a decrease in overall deposition efficiency will occur because of in-flight particle interactions and rebounding of the ceramic particles away from the substrate [26]. The overall deposition efficiency of pure nickel was low (~ 3%), however, once a small amount of WC was added to the mechanical blend, the overall deposition efficiency increased because the harder particles roughened the surface, thus improving the deposition efficiency of the metal. Once a limit of hard particles in the mechanical blend was met, a decrease in overall deposition efficiency was observed because the harder particles can erode the coating [27]. However, even though the overall deposition efficiency gradually decreased after 50 wt.% WC in the mechanical blend, there was an increase in WC deposition efficiency. This increase in WC content in the coating should ultimately improve the hardness and wear resistance of the coating.

Table 7: WC deposition efficiency and porosity of coatings

Mechanical blend	**WC deposition efficiency (%)**	**Overall deposition efficiency (%)**	**Coating porosity (vol.%)**
Nickel control	N/A	3	7 ± 0.2 (n = 3)
50WC + 50Ni	7 ± 0.9 (n = 9)	8	2 ± 0.7 (n = 9)
75WC + 25Ni	20 ± 1 (n = 10)	4	0.8 ± 0.2 (n = 10)
92WC + 8Ni	61 ± 1 (n = 12)	2	0.02 ± 0.005 (n = 9)
96WC + 4Ni	68 ± 0.5 (n = 12)	2	0.3 ± 0.1 (n = 12)

Table 7 also shows that as the WC content in the blend increased, the resulting coating porosity decreased. This phenomenon has also been observed by Koivuluoto *et al*. [25, 28] and Irissou *et al*. [23]. The decrease in porosity was due to the increased levels of impact by the harder WC particles onto the coating, increasing its density. The nickel control coating, which was devoid of WC

reinforcing particles, had the highest porosity of any fabricated coating. This is typical of cold-sprayed coatings that are fabricated from irregularly-shaped metal particles [28]. A dense region and a porous region was present in the cold-sprayed monolithic nickel coatings fabricated using 550°C and 92 psig, which was also present in the cold-sprayed monolithic nickel coatings fabricated using 475°C and 88 psig as seen in Fig. 20. Although porosity was present in the nickel coating, the impact of the nickel particles did improve the density of the coating because the porosity of the dense region and the porous region were 8 ± 0.7 vol.% and 15 ± 1 vol.%, respectively. This phenomenon was also observed in Section 3.1.3 when pure nickel was cold-sprayed at 475°C and 88 psig. It should be noted that averaging the porosities of the dense and porous regions will not give the overall porosity because magnified images will show smaller pores that may be difficult to see at lower magnifications. However, an image at low magnification that captures the entire coating is necessary to obtain an average porosity since the microstructure was non-homogeneous. Figure 28 shows magnified images of the WC-based MMC coatings that were fabricated by the 50 wt.% WC + 50 wt.% Ni and the 96 wt.% WC + 4 wt.% Ni mechanical blends. Along with Fig. 27, it can be concluded that the hard WC particles reinforce the nickel matrix of the MMC and improve the density of the coating further since there were fewer pores and gaps within the nickel matrix. The porous nature of the cold-sprayed nickel matrix may have been beneficial in this study because the WC-based particles can easily adhere to a porous layer due to the decreased resistance to plastic deformation by

the previously formed layer. This phenomenon was observed in other studies involving WC-Co coatings [18].

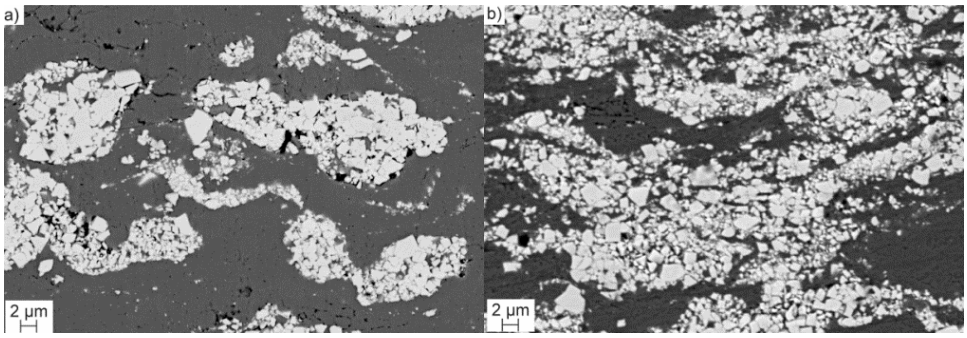

Figure 28: High magnification images of the WC-Ni MMC coatings fabricated from *a*) 50 wt. % WC + 50 wt. % Ni and *b*) 96 wt. % WC + 4 wt. % Ni

3.2.4 Vickers Micro-hardness[2]

Vickers micro-hardness indentations were conducted on the coatings to obtain a first order estimate of how the coatings will perform under abrasion. Although, hardness is not the sole indicator of the wear resistance of a coating, it is the simplest method of characterization. Figure 29 shows the effect of WC content on the micro-hardness of the coating. The figure shows that as the WC content in the coating increased, the micro-hardness increased as well. The 96 wt.% WC + 4 wt.% Ni powder blends produced the hardest coatings with a hardness of 533 ± 63 $HV_{0.3}$. The hardness was significantly higher than that of the cold-sprayed pure nickel coating at 137 ± 24 $HV_{0.3}$. This was expected because the coating hardness should increase when the content of the harder WC reinforcing particles increase.

[2] Portions of this section were published in: N. Melendez, A. McDonald, "Development of WC-based Metal Matrix Composite Coatings using Low-pressure Cold Gas Dynamic Spraying", *Surf. Coat. Technol.*, 214, 2013, 101 – 109.

Further, there was a reduction in porosity as the WC content increased in the coatings, which would also induce an increase in the hardness of the coating.

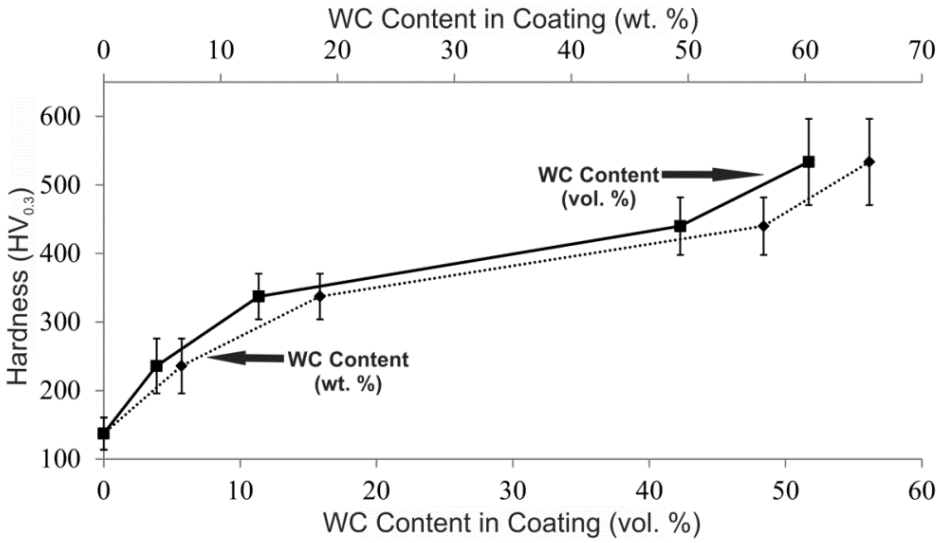

Figure 29: Curve of Vickers micro-hardness versus WC content in the coating

It is common for MMC coatings to have high standard deviations associated with their hardness (as seen in Fig. 29) because of the non-homogeneous distribution of ceramic or cermet particles in the fabricated coatings, along with the difference in hardness of the reinforcing particles and the matrix. Due to the low indentation load (300 gf) that was used, the indentations were often located in areas that contained a high concentration of WC particles or in areas that had mostly nickel matrix, which led to a high variation in hardness values. This effect has been observed in other studies [22, 23]. Finally, an increase in hardness was observed between the coatings fabricated from the 92 wt.% WC + 8 wt.% Ni and 96 wt.% WC + 4 wt.% Ni, without a significant increase in WC content in the fabricated coatings, as seen in Fig. 29. When coupled with Figs. 26c and 26d,

there was clear evidence that the non-homogeneous distribution of the reinforcing WC particles greatly influenced the hardness of the fabricated coatings.

Wang and Villafuerte [21] studied the hardness of WC-based MMC coatings that were fabricated by a cold spray unit operating at low pressure. The WC-based coatings were fabricated by using either 20 wt.% copper-coated WC particles or a 70 wt.% WC + 30 wt.% Cu mechanical powder blend. The maximum hardness values obtained for coatings fabricated from the Cu-coated WC particles and the mechanical blend were approximately 200 HB and 165 HB, respectively. In order to compare the coatings fabricated in this study to those fabricated in previous studies, ASTM Standard E140-2007 was used to convert Brinell hardness to Vickers hardness [72]. The Brinell to Vickers conversion chart for metals suggests that 200 HB is approximately equal to 200 HV and that 165 HB is approximately equal to 165 HV. An improvement in hardness of the 96 wt.% WC + 4 wt.% Ni MMC coatings was observed, and was approximately 2.5 times higher than that reported in a previous study [21]. The WC-based MMC coatings fabricated from the copper-coated WC particles contained approximately 55 vol.% of the reinforcing WC particles in the MMC coating, while those fabricated using the 70 wt.% WC + 30 wt.% Cu mechanical powder blend contained approximately 65 vol.% of the reinforcing WC particles in the MMC coating [21]. The coatings produced from the mechanical blends were not as homogeneous as those produced from the copper-coated WC particles, adversely affecting their overall hardness. The coatings fabricated from the WC-based mechanical blends in this present study contained a maximum of 52 ± 2 vol.% of reinforcing WC

particles. It can be concluded that the improved coating hardness of the 96 wt.% WC + 4 wt.% Ni was due, in part, to the presence of the harder nickel matrix because the MMC coatings fabricated from the 96 wt.% WC + 4 wt.% Ni powder blend had less WC reinforcing particles than those presented in the work of Wang and Villafuerte [21].

Although this study has shown an improvement in the hardness of WC-based MMC coatings in comparison to other low-pressure cold-sprayed WC-based coatings, the hardness values were still lower than those fabricated by HVOF spraying, PTA overlaying, and high-pressure cold spraying. The coatings in this study possessed a lower hardness than those fabricated by high-temperature processes (for example, HVOF spraying and PTA overlaying) because of a lower WC content in the coating and the lack of WC decarburization. Decarburization can cause WC to transform into W_2C. However, W_2C typically has a lower hardness (~1450 HV) [76] than WC (~1300 - 2400 HV) [17, 77]. The loss of carbon from the WC particles may allow the excess carbon to diffuse into the matrix, creating complex brittle secondary phases [29, 46]. These phases have been shown to degrade the coating by lowering its wear resistance [31, 46]. This suggests that the hardness of the coatings is not the only performance factor and that wear tests are necessary to compare the performance of HVOF coatings to low-pressure cold-sprayed coatings. High-pressure cold spraying was used to fabricate coatings with hardness values that were higher than the coatings presented in this study [17 - 19]. Coatings fabricated by high-pressure cold spraying have improved hardness because of a more uniform distribution of the

reinforcing WC particles in comparison to coatings fabricated in this study. A more uniform distribution can be obtained by spraying powders that are agglomerated rather than mechanically blended or by post-treatments, such as friction stir processing (FSP). FSP is a derivative of friction stir welding, where a tool piece is used to enhance the surface properties by frictional heating, plastic deformation, and redistributing reinforcing particles [22, 78]. Hodder *et al*. [22] have shown that the hardness of cold-sprayed Al/Al_2O_3 MMC coatings was improved when the hard Al_2O_3 particles were evenly distributed by a FSP tool.

Although the hardness values were lower than that which is typical for thermal-sprayed WC-Co coatings, it was important to approximate the mechanical properties of MMCs for materials application. The simplest method to estimate the properties of a composite is through the rule of mixtures (ROM) [79]. ROM suggests that the mechanical properties of the composites often lie between iso-stress (Reuss) conditions and iso-strain (Voigt) conditions. Iso-stress conditions are those in which the stress is equal throughout the composite medium, while iso-strain conditions represent equal strain throughout the medium. Chang *et al*. [80] and Hodder *et al*. [22] found that MMCs whose reinforcing particles were uniformly redistributed by FSP had hardness values closer to iso-stress values. The empirical equations for the equal stress (iso-stress) and equal strain (iso-strain) conditions are shown in Eqs. 6 and 7, respectively:

$$\overline{H}_{\text{low}} = (f_{\text{h}}/H_{\text{h}} + f_{\text{s}}/H_{\text{s}})^{-1}, \tag{6}$$

$$\overline{H}_{\text{upper}} = f_{\text{h}}H_{\text{h}} + f_{\text{s}}H_{\text{s}}, \tag{7}$$

where, $\overline{H}$ is the effective hardness of the composite, H_h and H_s are the hardness values of the hard and soft phases, respectively, and f_h and f_s are the volume fractions of the hard and soft phases, respectively. The subscripts "upper" and "lower" on $\overline{H}$ represent the upper and lower bounds, respectively. The hardness of the reinforcing WC-based particles was taken as 2350 HV because that is the hardness of pure WC [81]. It should be noted that the hardness of bulk WC can range between approximately 1300 and 2400 HV, depending on the crystal orientation [17, 77], which would have an effect on the overall hardness of the fabricated coating. The cobalt present in the WC-based reinforcing particles was neglected because its content was low (12 wt.%) and is much softer than WC, having a negligible effect on the overall hardness of the hard reinforcing particles. The hardness of the soft phase, nickel, was taken to be 137 HV, which was the hardness of the cold-sprayed nickel coating.

Table 8 presents the lower and upper bounds of the predicted hardness values for each composite coating, along with the experimental hardness values. All the coatings, except that fabricated from the 50 wt. % WC + 50 wt. % Ni powder blend, were between the predicted hardness limits established by the empirical relations of Eqs. 6 and 7. The standard deviations of the WC coating content were relatively low in comparison to the average WC content in the coating, with the exception of the coating fabricated using the 50 wt.% WC + 50 wt.% Ni mechanical blend. It was clear that a small change in WC content in the coating has a great effect on the upper hardness limit. Therefore it is important to understand that the hardness limits were based on the average WC content in the

coating and that the high standard deviation, in comparison to the average, of the coating fabricated using the 50 wt.% WC + 50 wt.% Ni mechanical blend may be the reason the experimental hardness was not in between the two hardness limits suggested by ROM. However, in general these coatings behaved similarly to MMC coatings produced by other investigators [22, 80].

Table 8: Predicted upper and lower hardness values and experimental hardness values of WC-based MMC coatings

Mechanical blend	**WC content in coating (vol. %)**	**Experimental hardness ($HV_{0.3}$)**	H_{low} **(HV)**	H_{upper} **(HV)**
50WC + 50Ni	4 ± 2	236 ± 40	142	223
75WC + 25Ni	11 ± 2	337 ± 33	153	389
92WC + 8Ni	42 ± 4	440 ± 42	227	1073
96WC + 4Ni	52 ± 2	533 ± 63	265	1281

Kim [82] proposed that composites generally follow the iso-strain behaviour, provided that the reinforcing particle content in the coating is high. For low reinforcing particle content, an iso-stress condition is followed. This trend was explained by load sharing, where deformation of the softer matrix is much larger than that of the hard reinforcing particles. If the volume content of the reinforcing phase is high, then the load can be distributed to other reinforcing particles to produce reduced deformation in the overall composite. If the volume content of the reinforcing particles is low, then the soft matrix will deform, resulting in a lower hardness. The behaviour proposed by Kim [82] was not observed in this present study for the coatings that contained 4 vol.% WC and 11 vol.% WC because their model did not consider plastic deformation of the matrix, adiabatic shear instabilities, and coating porosity. For the coatings that possessed a low

volume content of WC particles, for example 4 vol.% WC, the average hardness was closer to the iso-strain condition. Cold spraying fabricates refined coatings by inducing adiabatic shear instabilities, work hardening, and dynamic recrystallization, where improvements in hardness have been observed throughout the coating at the particle-substrate interfaces [12, 73, 74]. In this study, the hardness of commercially pure annealed nickel is approximately 79 HB [71], which is approximately 79 HV, according to ASTM Standard E140-2007 [72]. The hardness of the cold-sprayed pure nickel control coating was 137 HV and that of the coating containing 4 vol.% WC was 236 HV. Cold working of the Ni matrix, which was not considered by Kim [82] in their model, was sufficient to produce iso-strain conditions in coatings with low WC content.

Low-force (10 gf) Vickers micro-hardness indents were also conducted on the matrix near the carbide and on the matrix, far from the carbides to determine if the impact of the WC particles improved the hardness locally. A low force was used to minimize the effects of the WC-based particles that may be underneath the exposed surface and nearby WC-based particles. The latter would have an effect if the indent force is higher because it will create a large indent which may cause the indent to feel the effects of nearby carbides seen on the exposed surface. Therefore, when taking these limitations into consideration, the coating that contained 4 vol.% WC was used to conduct the low-force Vickers micro-hardness indents. Figure 30 shows a micrograph of an indent that was taken on the matrix near the carbide. The indent was located below the carbide because that area was expected to have increased hardness due to the impact of the hard, reinforcing

WC-based particle during deposition. Figure 31 shows a micrograph where the indent was taken in the nickel matrix where there were no carbides in close proximity. The hardness of the matrix near the carbide was 311 ± 91 $HV_{0.01}$, while the hardness of the matrix away from carbides was 281 ± 54 $HV_{0.01}$. A t-test assuming unequal variances was used to compare the two average hardness values. A t-test was used due to the low amount of indents conducted [83], $n = 10$, for both locations. Unequal variances were assumed because there was not enough evidence to assume equal variances of the two different areas. The t-test determined that there was no significant statistical difference between the two means. This suggests that the impact of the WC-based particles did not locally enhance the hardness; however, the presence of the reinforcing particles did improve the hardness of the overall coating. A detailed t-test sample calculation can be found in Appendix A.

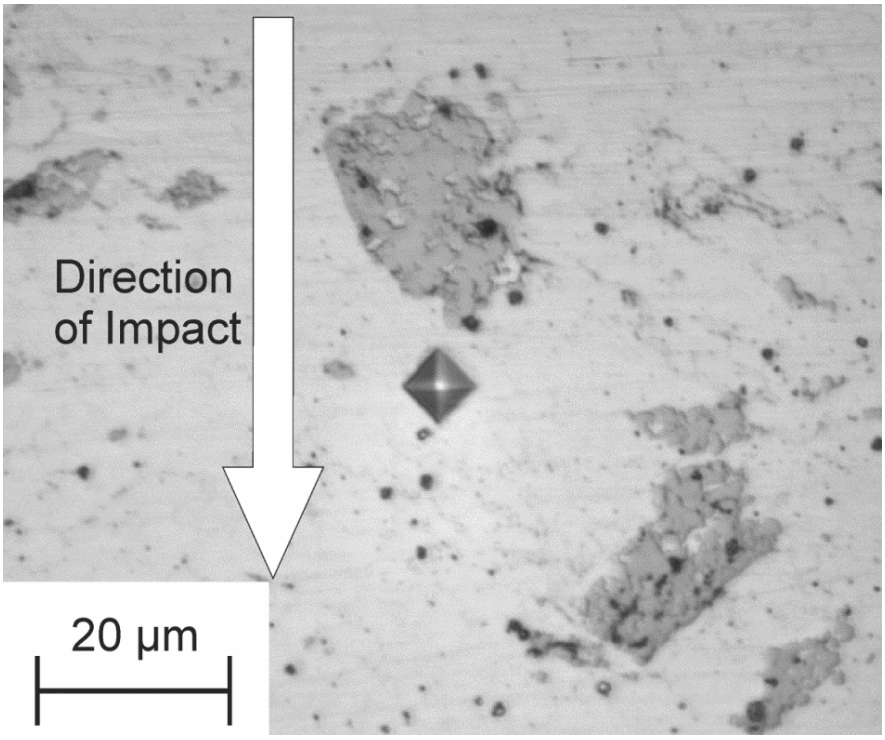

Figure 30: Low-force hardness indentation on matrix near carbide

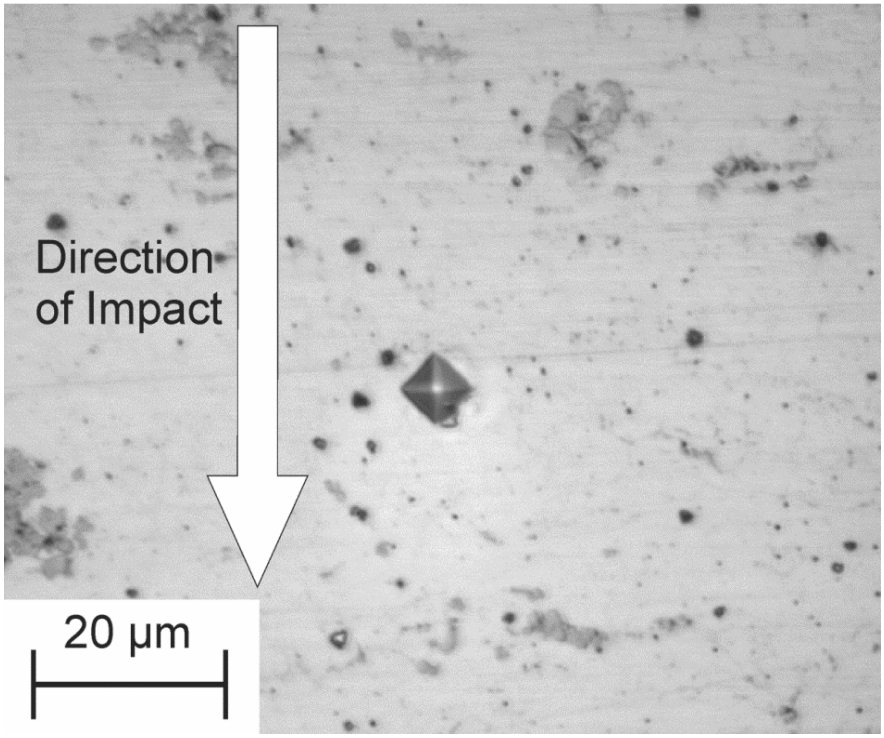

Figure 31: Low-force hardness indentation on matrix away from carbides

3.2.5 Relationship between Hardness and Wear Rate[3]

Hardness indentations are typically conducted on materials to gain an understanding of how the material will perform during wear. However, there is often no simple correlation between hardness and wear rate for MMC coatings because toughness has an effect on the coating's ability to resist wear [3, 42, 44, 58 - 60]. Figure 32 shows the effect of hardness on the wear rate of each MMC coating. As the hardness of the WC-based MMC coating increased, the wear rate decreased. The wear rate of nickel was not presented because it had a wear rate of approximately 1.2 x 10^{-3} mm^3/Nm, which was an order of magnitude higher than the highest wear rate of each WC-based MMC coating explored in this study. Each data point in the figure is also shown with the WC content in the coating in wt.% and vol.%. The relationship between hardness and wear rate for the WC-Ni MMC coating was relatively linear. This suggests that hardness was a crucial property that contributed to the wear resistance of these cold-sprayed MMC coatings and could be used to approximate the wear rate of this MMC system. The difference in the slope at a lower WC content may be due to a change in porosity because it was determined that the porosity decreased when the WC content increased in the coating. This would further decrease the wear rate of the coatings. Zhao *et al*. [40] found that porous HVOF-sprayed WC-CoCr coatings had a higher wear rate than dense HVOF-sprayed WC-CoCr coatings. Although,

---

[3] Portions of this section were published in: N. Melendez, V. Narulkar, G. Fisher, A. McDonald, "The Effect of Reinforcing Particles on the Wear Rate of Low-pressure Cold-sprayed WC-based MMC Coatings", *Wear*. Under review.

hardness could be used as a first-order approximation of the wear rate of these WC-based MMC coatings, the coating toughness will also have an effect on the wear resistance. However, quantifying the toughness of the MMC coatings would be difficult due to the small dimensions of the coating and the higher thickness requirements for conventional tests for metals/alloys. Further, limited crack generation occurred at the hardness indentations due to the high ductility of the nickel metal matrix. The standard deviations of the wear rates were not presented in Fig. 32 because only two wear tests were conducted on each coating of a given composition. However, the difference between the two wear rate values of the coatings never exceeded 7 x 10^{-6} mm^3/Nm, suggesting that there was small variation between the wear-tested coatings.

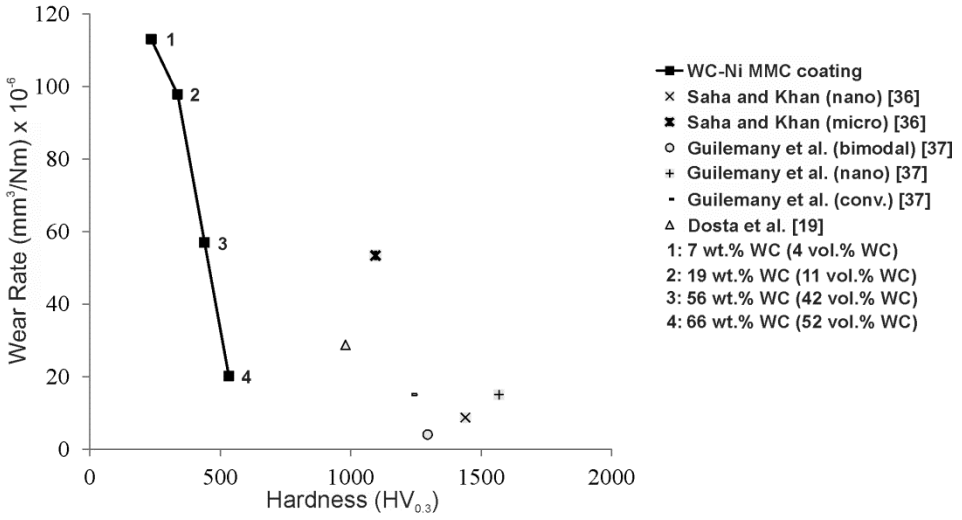

Figure 32: Curve of wear rate versus hardness, showing the respective WC content in the coating

Although the wear rate of the cold-sprayed MMC coatings decreased as the WC content in the coating increased, it was important to compare the wear rate of

these coatings to WC-based coatings fabricated by HVOF spraying and high-pressure cold spraying. Figure 32 compares the wear rates of the various WC-Ni MMC coatings fabricated by using low-pressure cold spraying to those of various HVOF-sprayed and high-pressure cold-sprayed WC-Co coatings. Saha and Khan [36] and Guilemany *et al*. [37] fabricated WC-Co coatings using HVOF spraying and subjected them to dry abrasion testing (ASTM G65), using similar parameters as in this study, with variations of the silica (SiO_2) feed rate, the amount of revolutions, or the applied force. However, the difference in SiO_2 feed rate should not have a significant effect on the wear rate of the coating because the ASTM G65-2004 standard states that the sand flow rate must be between 300 g/min and 400 g/min [67]. Furthermore, a difference in test revolutions will not affect the wear rate of the coating provided that the coatings do not exhibit severe phase segregation. Nahvi *et al*. [84] also showed that surfaces with high hardness that were exposed to low loads behave similarly to softer surfaces that had a high applied load during the dry sand-rubber wheel test. The low-pressure cold-sprayed MMC coating that contained 66 wt.% WC had a wear rate that was higher than each HVOF-sprayed WC-Co coating to which it was compared, with the exception of the microcrystalline WC-17Co coating fabricated by Saha and Khan [36]. The microcrystalline WC-17Co coating likely had a higher wear rate because of higher coating porosities, higher levels of decarburization, and lower toughness, when compared to the near-nano-crystalline WC-Co coating [36]. Although a higher hardness (~1100 HV) and a higher WC content (83 wt.% WC) was achieved in the HVOF-sprayed microcrystalline WC-Co coatings, they

showed higher wear rates than those of the low-pressure cold-sprayed MMC coatings that contained 66 wt.% WC, which indicated the negative impact of WC decarburization. The formation of detrimental phases due to decarburization led to embrittlement of the HVOF-sprayed WC-17Co coatings, while the ductility and toughness are retained in the nickel matrix of the low-pressure cold-sprayed WC-based MMC coatings since no chemical changes occurred after cold spray deposition. This confirmed that hardness is not always the sole indicator of the performance of a coating during wear applications, especially when a larger amount of non-ductile phases are present.

In order to eliminate decarburization, cold spraying can be used to fabricate WC-based MMC coatings. Dosta *et al*. [19] successfully fabricated WC-25Co cermet coatings onto steel substrates and subjected them to ASTM G65 dry abrasion wear testing. Figure 32 shows that the WC-based MMC coating fabricated using low-pressure cold spraying that had a 66 wt.% WC content had a comparable wear rate to that of the WC-25Co coatings fabricated using high-pressure cold spraying, although the WC-25Co coatings had a higher hardness. The higher hardness was likely due to the more homogeneous distribution of WC-Co grains, in comparison to the coatings fabricated by low-pressure cold spraying. However, it appeared that the distribution of the WC-Co particles had a negligible effect on the overall wear rate of the fabricated coatings. Furthermore, both coatings had nearly the same WC content, approximately 66 wt.% WC in the optimized WC-based MMC coating versus 75 wt.% WC (WC-25Co) in the high-pressure cold-sprayed coatings, with neither of the coating systems exhibiting

signs of decarburization. The similarities in the microstructures of both coatings led to comparable wear rates, suggesting that low-pressure cold-sprayed WC-based MMC coatings could be used as a low-cost alternative.

3.2.6 Effect of Mean Free Path on Mechanical Properties[4,5]

The mean free path between the reinforcing particles can be used to explain the strengthening effects of the WC-based particles on the coating. Kouzeli and Mortensen [62] have shown that the mechanical properties of composites improved when the mean free path of the reinforcing particles decreased. Figure 33 shows the relation between WC content in the coating and the mean free path between the WC particles in the coating. As the WC content in the coating increased, the mean free path decreased, as suggested by Eq. 1. The coatings that had the highest amount of WC-based reinforcing particles had the lowest mean free path. From the trend exhibited in Fig. 33, it was expected that the coatings with the highest WC content should have the optimum mechanical properties. Figure 34 shows a relationship between the mean free path and the hardness of the WC-based MMC coatings. The coatings fabricated from the 96 wt.% WC + 4wt.% Ni powder blend had the highest hardness of 533 ± 63 $HV_{0.3}$, which was due, in part, to the low mean free path between the WC reinforcing particles.

---

[4] Portions of this section were published in: N. Melendez, A. McDonald, "Development of WC-based Metal Matrix Composite Coatings using Low-pressure Cold Gas Dynamic Spraying", *Surf. Coat. Technol.*, 214, 2013, 101 – 109.

[5] Portions of this section were published in: N. Melendez, V. Narulkar, G. Fisher, A. McDonald, "The Effect of Reinforcing Particles on the Wear Rate of Low-pressure Cold-sprayed WC-based MMC Coatings", *Wear*. Under review.

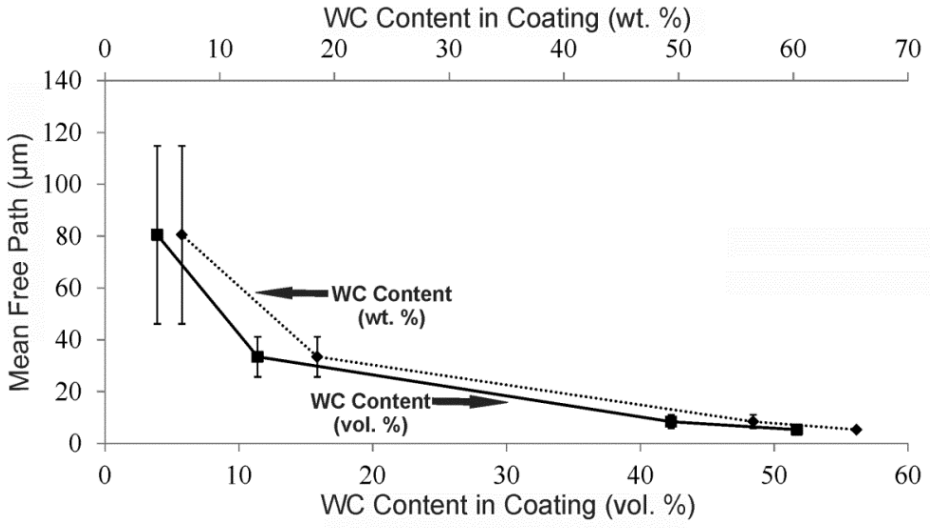

Figure 33: Relationship between mean free path between the WC particles and the WC content in the coating

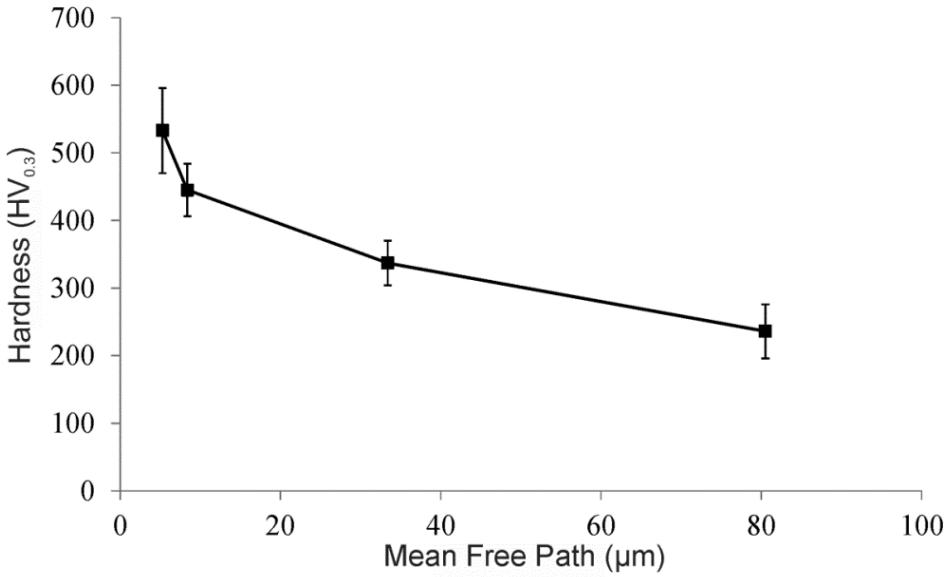

Figure 34: Curve of hardness versus mean free path

Figure 35 shows the effect of mean free path on the wear resistance of the cold-sprayed WC-based MMC coatings. As the mean free path decreased, the wear rate decreased. Interestingly, the relationship between the mean free path and the wear rate was not linear. At larger mean free paths, a decrease in the mean free path did

not improve the wear resistance as much as it did at lower mean free paths. This could be due to the rounded and irregular morphology of the SiO_2 particles (see Fig. 8). The diameter of the abrasives was between 212 – 300 μm. Due to their large, irregular shape, the abrasives may have easily worn the portions of the nickel matrix that were not reinforced by the WC-based particles. This may support the observation that the coatings with higher mean free path distances between the reinforcing WC particles had higher wear rates. Reduction of the mean free path between the reinforcing hard particles likely reduced the probability of interaction between the SiO_2 abrasive particles and the softer Ni metal matrix, reducing the overall wear rate of the MMC coating. It was unlikely that the SiO_2 abrasive particles had asperities smaller than approximately 10 μm, which represents the approximate mean free path value at which significant improvements in the wear performance of the low-pressure cold-sprayed WC-based MMC coatings were observed. This would make the interaction between the hard abrasives and the softer nickel matrix less likely, thus improving the wear rate of the WC-based MMC coatings. Also, Kouzeli and Mortensen [62] observed a great improvement in mechanical properties when the mean free path decreased to values below 10 μm, which was observed for both the hardness and wear rate of the WC-based MMC coating system.

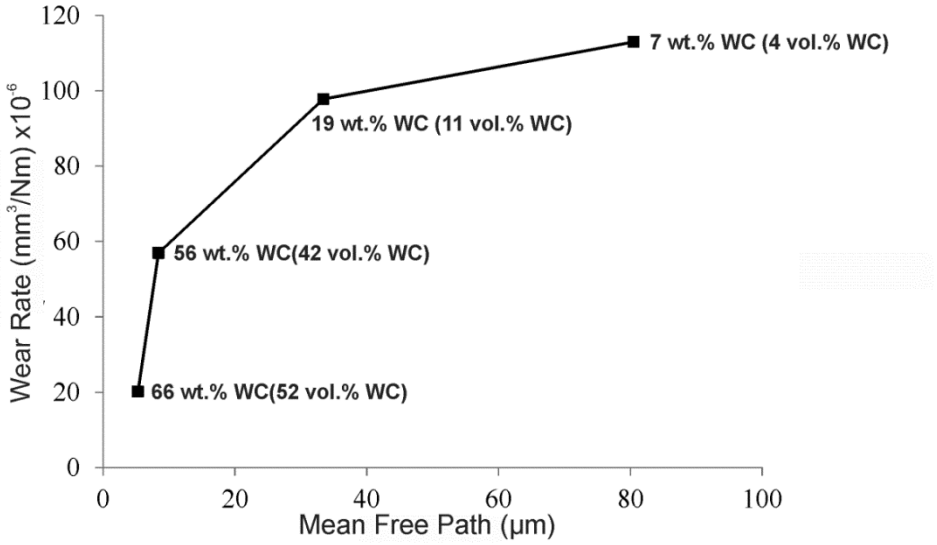

Figure 35: Curve of wear rate versus mean free path

3.2.7 X-ray Diffraction (XRD)[6]

XRD analysis was used to determine the materials and phases that were present in both the mechanical powder blends and the fabricated coatings. Figure 36 shows the XRD profiles of the mechanical blends at a composition of 96 wt.% WC + 4 wt.% Ni. The XRD profile showed that only a WC and a nickel phase were present in the mechanical blend. The cobalt binder in WC was not detected using XRD analysis. This was most likely due to the low amount of cobalt present in the WC-based powder, which supports the assumption of negligible effect of cobalt on the density of the overall coating. Figure 37 shows the XRD profiles of the WC-based MMC coatings that were fabricated from the various compositions of mechanical blends. None of the coatings exhibited signs of decarburization or oxidation after deposition because WC and nickel were the only phases present.

[6] Portions of this section were published in: N. Melendez, A. McDonald, "Development of WC-based Metal Matrix Composite Coatings using Low-pressure Cold Gas Dynamic Spraying", *Surf. Coat. Technol.*, 214, 2013, 101 – 109.

This result was expected because the pseudo-binary WC-Co phase diagram and the W-C phase diagram suggest that phase changes should not occur below approximately 1250°C [49, 50]. The use of compressed air at a temperature of 550°C along with the short residence time of the particles in the working fluid reduced the possibility of any phase transformations or chemical changes.

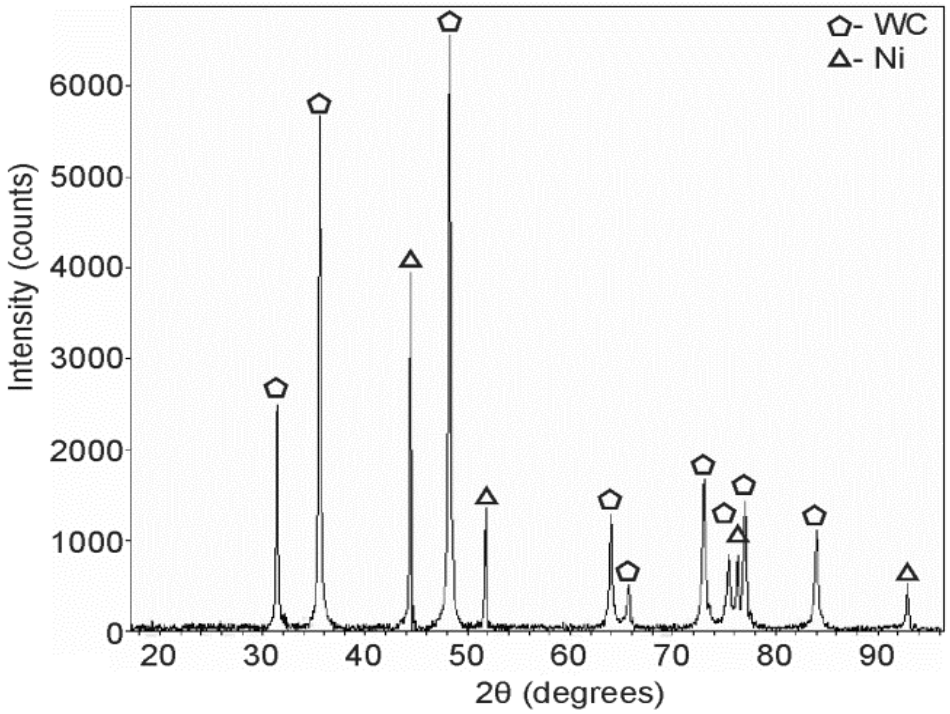

Figure 36: XRD profiles of the 96 wt.% WC + 4 wt.% Ni mechanical powder blend

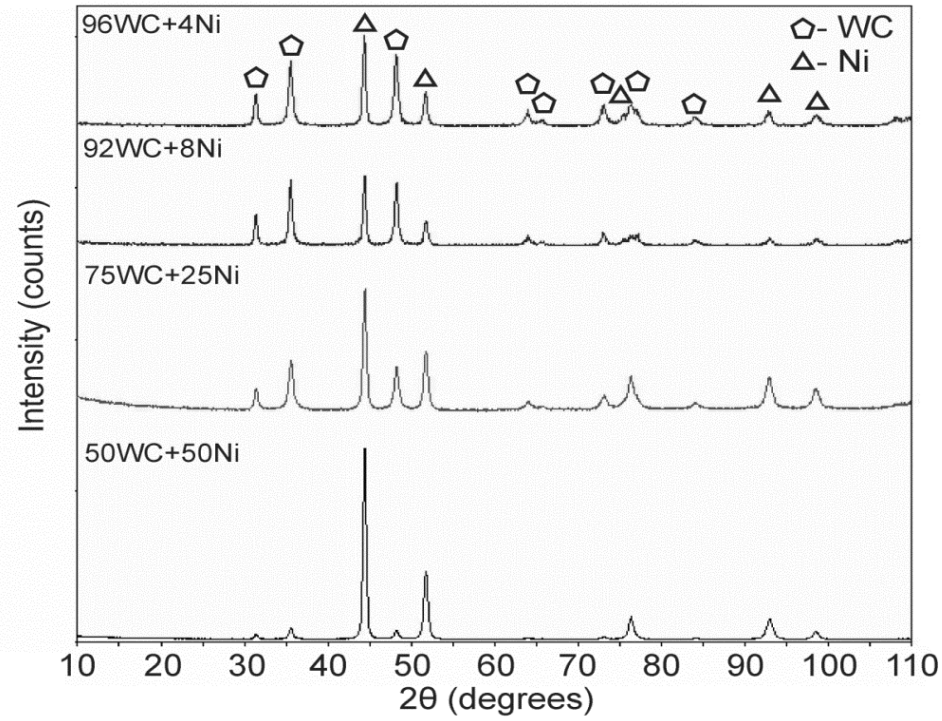

Figure 37: XRD profiles of the cold-sprayed WC-based MMC coatings

XRD also provides a relative comparison of the amount of material that is present in a given mixture. The primary peaks of WC and Ni are at 2θ angles of approximately 48° and 44°, respectively. Figure 37 show that when the WC content in the powder blend increased, there was a relative increase of the primary peak of WC in comparison to the primary peak of Ni for the coatings. These results agreed with those obtained from the ImagePro software for the vol.% of WC in each coating (see Fig. 27). Each XRD profile showed a large amount of Ni present in each of the fabricated coatings because the primary Ni peak was nearly as high as or higher than the primary WC peak. In addition, there was a significant increase in the primary nickel peak for the XRD profiles of the coating fabricated from the 96 wt.% WC + 4 wt.% Ni powder blends (see Fig. 37) in comparison to the 96 wt.% WC + 4 wt.% Ni mechanical powder blends shown in

Fig. 36. This occurred because the softer nickel particles were deposited easier than the harder WC particles into the coating. This trend has been observed in other studies that involved fabrication of MMC coatings via low-pressure cold spraying [22, 23, 26]. Agglomerating the WC particles with a soft metal would ensure that a lower amount of metal would be in the coating. Agglomeration of the WC particles with nickel would also produce a homogeneous coating because the individual carbides would be more evenly dispersed throughout the coating. Careful design of the powder will be necessary because large metal binder content in the powder will decrease the hardness and low binder content will cause the cermet agglomerate powder to rebound from the substrate surface.

3.2.8 Case Study: Comparison to Pure WC + Ni (p-WC+Ni) MMC Coatings

Pure WC + Ni (p-WC+Ni) MMC coatings were fabricated using an inexpensive pure WC powder to determine the possibility to fabricate coatings with similar hardness values. SEM images were not presented because the microstructures of the coatings were very similar to those that were fabricated in the WC-Ni system. Figure 38 plots the hardness values and WC coating content of both the p-WC+Ni MMC and WC-Ni MMC coatings. The error bars presented are one standard deviation. The numbers above the error bars of the p-WC+Ni MMC coatings data points denote the mechanical blend composition used to fabricate that coating. 96 wt.% WC + 4 wt.% Ni was chosen because that was the mechanical blend composition that produced the hardest WC-Ni MMC coating. However, the coating fabricated using the 96 wt.% p-WC + 4 wt.% Ni blend did not contain the same reinforcing particle content as the coatings fabricated using

the 96 wt.% WC + 4 wt.% Ni blend (see Figs. 27 and 38). With that result, two more mechanical blend compositions (98 wt.% WC + 2 wt.% Ni and 99 wt.% WC + 1 wt.% Ni) were explored to determine if deposition was possible. It was possible to fabricate the coatings; however, it was not possible to fabricate them with WC content similar to that of the highest WC content from the WC-Ni system. Furthermore, there was a slight deviation from the curve generated from the WC-Ni hardness results.

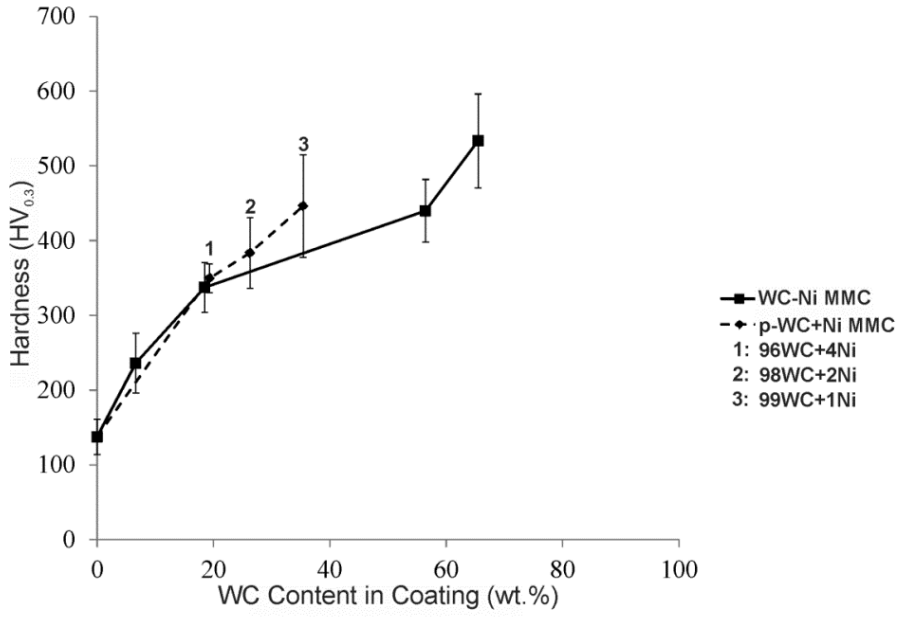

Figure 38: Curve of hardness versus WC coating content for p-WC+Ni and WC-Ni coatings

The mean free path between the reinforcing WC particles was measured and used to explain the slight deviations in hardness and WC coating content. Figure 39 compares the fabricated p-WC+Ni coatings to the WC-Ni coatings, with respect to their hardness and mean free path. Figure 39 shows that the mean free path can be used to predict the hardness of any WC-based-Ni coating because the

curves shown in the figure for the two different systems agree well and nearly coalesce. Furthermore, this suggests that the cobalt present in the WC-Co reinforcing particles had a negligible effect on the coating, which supports the assumption that cobalt has a negligible effect on coating density and coating hardness.

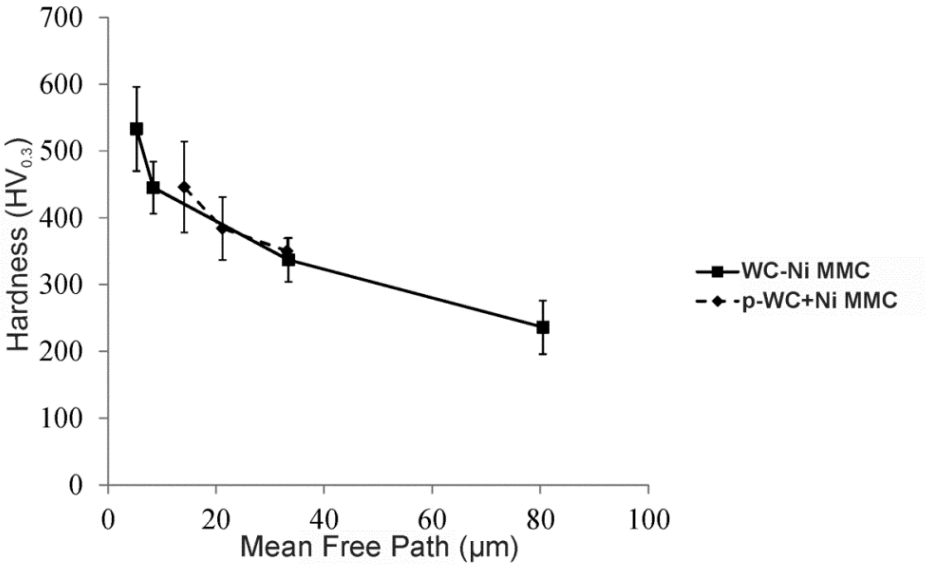

Figure 39: Curve of Hardness versus mean free path for p-WC+Ni and WC-Ni coatings

4. Conclusions

The first phase of this study served to explore the feasibility of depositing WC-based MMC coatings by low-pressure cold spraying various WC-Ni-Cu mechanical powder blends. The cold spray parameters were optimized to fabricate coatings that had the highest WC coating content and the highest hardness. The coatings fabricated from 96 wt.% WC + 2 wt.% Ni + 2 wt.% Cu mechanical blend powders had the highest WC content and the highest hardness. EDS was used to confirm which phases were present in the coating, while XRD analysis confirmed that no decarburization of the WC-based particles or oxidation of the binder metals occurred during or after deposition. Furthermore, the XRD profiles suggested that the copper content (the softest phase) was too high when compared to the WC content. The average coating hardness was not comparable to those obtained by HVOF and high-pressure cold-sprayed coatings; therefore, it was decided to remove copper from the mechanical blends before any wear tests were conducted.

The second phase of this study was to fabricate WC-Ni MMC coatings; however, since nickel is not as soft as copper, the cold spray parameters were modified slightly to promote deposition of nickel. Different compositions of mechanical blends were used to fabricate different MMC coatings. The WC-based MMC coatings were characterized using SEM coupled with image analysis, EDS, XRD, and Vickers micro-hardness indentations. Furthermore, ASTM standard G65-2004 tests were conducted on this coating system because of the improved

coating hardness in comparison to the WC-Ni-Cu MMC coatings. Image analysis was used to determine the WC content in each fabricated coating and the mean free path. The mean free path was used to explain the improvement in mechanical properties and to compare the properties of the coatings that used different WC-based particles in the mechanical blends. The 96 wt.% WC + 4 wt.% Ni mechanical powder blend produced the coating with the highest hardness and lowest wear rate. ROM was used to predict the hardness of the various WC-Ni MMC coatings. However, ROM did not accurately describe the mechanical properties because of the coating porosity, adiabatic shear instabilities, work hardening, and dynamic recrystallization, which will have an effect on the mechanical properties of the cold-sprayed WC-based MMC coatings. Also, none of the fabricated coatings of both WC-Ni systems exhibited decarburization or oxidation. It was determined that the wear rate was linearly correlated to the coating hardness. It was necessary to compare the wear rate of the optimized coatings fabricated by the WC-Ni mechanical blends to typical WC-based coatings fabricated via HVOF and high-pressure cold spraying. It was observed that the optimized low-pressure cold-sprayed coatings had comparable wear rates despite the large difference in hardness. This was due to decarburization, which created brittle phases. However, the wear rate of the low-pressure cold-sprayed MMC coatings was generally higher because of the lower WC coating content in comparison to HVOF-sprayed WC-12Co coatings. The wear rate of the low-pressure cold-sprayed WC-Ni coatings were comparable to the wear rate of WC-25Co coatings fabricated using high-pressure cold spraying because both coatings

did not exhibit signs of decarburization or oxidation and the coatings had a similar WC content.

The third and final stage of this study was to compare the coating hardness of WC-Ni MMC coatings that contained pure WC particles or WC-12Co particles. It was not possible to fabricate coatings with the same WC content when using the same mechanical blend composition. The p-WC+Ni MMC coatings had slightly higher hardness values than the WC-Ni MMC coatings. However, the relationship between the mean free path of the reinforcing particles and hardness were the same for both the WC-Ni and p-WC+Ni MMC coating systems, suggesting that cobalt had a negligible impact on the coating properties.

From this study, it has been shown that it is possible to fabricate thick WC-based MMC coatings using low-pressure cold spraying. Furthermore, these coatings can be used as an alternative option that yields similar wear rates to those of HVOF and high-pressure cold-sprayed coatings.

5. Future Work and Recommendations

The focus of this study was to fabricate WC-based MMC wear resistant coatings using a low-cost, low-pressure cold spray unit. The cold spray parameters were varied and the resulting coatings were characterized, while the optimized coatings were subjected to dry abrasion testing. A relationship between hardness and wear rate of the coatings was determined. However, surface wear scar and cross-sectional wear scar analysis must be conducted to gain an understanding of the mechanisms of wear and material removal from the WC-Ni MMC coatings. Furthermore, material removal and wear rates must be explained through accepted models.

There are additional tests that may be conducted to understand how these MMC coatings can be applied. First, ASTM Standard C633-2001 should be conducted to determine the bond strength of the coating. Although the coatings were still intact with the substrates after wear testing, it is crucial to quantify the bond strength to ensure the coatings will not peel off in other applications. Preliminary tests were conducted to gain understanding of the bond strength; however, detailed testing and analysis were outside of the scope of this study. The preliminary results are shown in Table 9.

Table 9: Preliminary ASTM C633-2001 results

Mechanical blend composition	**WC content in coating (wt.%)**	**Adhesion/cohesion strength (MPa)**
96wt.% WC + 4 wt.% Ni	66 ± 2 (n = 12)	19 ± 4 (n =2)

Other tests that were not explored in this study, but may be critical to understand further these coatings are corrosion testing and B611-85, to name a few. Corrosion testing is necessary to determine how the coating will perform in a strictly corrosive condition that is typically observed in the oil and gas industry. Also, ASTM B611-85(2005) tests should be conducted to understand the wear mechanisms when the coatings are subjected to wet abrasion applications, where corrosion may also occur.

A significant amount of coating characterization was conducted on the as-sprayed WC-based MMC coatings, however, the grain boundaries of the nickel matrix were never measured. Attempts were made at etching the nickel matrix with Marble's reagent (10g $CuSO_4$: 50 mL HCl: 50 mL water) and 3% nital (3 mL HNO_3 : 97 mL ethanol). Neither etchants exposed the grain boundaries of the nickel matrix, but severely over-etched the steel substrate. Attempts at etching the feedstock nickel powder were unsuccessful as well. Other etchants should be explored if one desires to determine if any grain refinement occurred in the nickel matrix after cold spraying with or without the WC-based particles.

Although the wear rates were comparable to those of coatings fabricated by HVOF and high-pressure cold-spraying, thermal-sprayed coatings can have wear rates that are comparable to bulk WC-Co hardmetals [3]. Post-treatments such as FSP should be examined to refine the coating microstructure and redistribute the hard reinforcing particles. Studies have shown that using FSP improves the hardness of thermal-sprayed coatings [22, 78, 85]. However, no studies have measured the wear rates of thermal-sprayed coatings that were subjected to

friction-stir processing. The improvement in hardness should yield an improvement in wear rate, provided that no phase transformations or chemical changes occur.

Although high-temperature processes typically cause coatings to exhibit signs of decarburization, flame spraying could be used to fabricate WC-based MMC coatings. If the WC-based powder is mechanically blended with a powder with a eutectic composition, a lower flame temperature could be used and still melt or soften the matrix while minimizing or eliminating decarburization of the WC-based particles. Eutectic systems like Ni-4 wt.% B or Al-12 wt.% Si could be used because of their lower melting points to improve deposition. If porosity is too high, post-treatments such as heat treatment and fusing could improve the properties of the coatings. A similar study was conducted by Kim *et al*. [86] where WC-12Co powder was mechanically blended with various nickel powders and the resultant coatings were heated in a furnace to reduce the inter-particle porosity.

Finally, it is necessary to deposit the coatings onto small pieces of equipment that are subjected to aggressive wear environments, such as mud valves that are used in down-hole drilling in the oil and gas industry. Experimental tests can give an idea of how the coatings will perform and can be used to compare and evaluate different coatings; but field tests subject the coatings to the true environment that can often be difficult to replicate in experiment. The equipment can be examined both macroscopically and microscopically, if failure occurs, to understand the failure mechanisms in an attempt to improve the coatings further.

6. References

1. F. Rastegar, D.E. Richardson, Surf. Coat. Technol. 90 (1997) 156-163.

2. Š. Houdková, F. Zahálka, M. Kašparová, L.-M. Berger, Tribol. Lett. 43 (2011) 139-154.

3. S.F. Wayne, S. Sampath, J. Therm. Spray Technol. 1(4) (1992) 307-315.

4. L. Pawlowski, The Science and Engineering of Thermal Spray Coatings, second ed., John Wiley & Sons, Chichester, UK, 2008.

5. ASM International, Handbook of Thermal Spray Technology, Thermal Spray Society Training Committee, 2004, ASM, p 5-9.

6. P. Fauchais, G. Montavon, Key Engineering Materials 384 (2008) 1-59.

7. A. Papyrin, Adv. Mater. Proc. 159(9) (2001) 49-51.

8. M. Grujicic, C.L. Zhao, W.S. DeRosset, D. Helfritch, Mater. Des. 25 (2004) 681-688.

9. H. Assadi, F. Gärtner, T. Stoltenhoff, H. Kreye, Acta Mater. 51 (2003) 4379-4394.

10. T. Schmidt, F. Gärtner, H. Assadi, H. Kreye, Acta Mater. 54 (2006) 729-742.

11. Y. Zou, D. Goldbaum, J. Szpunar, S. Yue, Scr. Mater. 62 (2010) 395-398.

12. M.P. Dewar, A.G. McDonald, A.P. Gerlich, J. Mater. Sci. 47 (2012) 184-198.

13. “Cold Spray”, Thermal Spray Technologies Inc., Accessed December 17, 2012. Available: http://www.tstcoatings.com/cold_spray.html.

14. E. Irissou, J.-G. Legoux, A. Ryabinin, B. Jodoin, C. Moreau, J. Therm. Spray Technol. 17(4) (2008) 495-516.

15. R.S. Lima, J. Karthikeyan, C.M. Kay, J. Lindemann, C.C. Berdnt, Thin Solid Films 416 (2002) 129-135.

16. P.H. Gao, C.J. Li, G.J. Yang, Y.G. Li, C.X. Li, Appl. Surf. Sci. 256 (2010) 2263-2268.

17. H.J. Kim, C.H. Lee, S.Y. Hwang, Surf. Coat. Technol. 191 (2005) 335-340.

18. P.H. Gao, Y.G. Li, C.J. Li, G.J. Yang, C.X. Li, J. Therm. Spray Technol. 17(5-6) (2008) 742-749.

19. S. Dosta, M. Couto, J.M. Guilemany, Acta Mater. 61 (2013) 643-652.

20. C.J. Li, G.J. Yang, P.H. Gao, J. Ma, Y.Y. Wang, C.X. Li, J. Therm. Spray Technol. 16(5-6) (2007) 1011-1020.

21. J. Wang, J. Villafuerte, Adv. Mater. Proc. 167(2) (2009) 54-56.

22. K. Hodder, H. Izadi, A. McDonald, A. Gerlich, Mater. Sci. Eng. A 556 (2012) 114-121.

23. E. Irissou, J.G. Legoux, B. Arsenault, C. Moreau, J. Therm. Spray Technol. 16(5-6) (2007) 661-668.

24. D. Poirier, J.G. Legoux, R.A.L. Drew, R. Gauvin, J. Therm. Spray Technol. 20(1-2) (2011) 275-284.

25. H. Koivuluoto, J. Lagerbom, M. Kylmälahti, P. Vuoristo, J. Therm. Spray Technol. 17(5-6) (2008) 721-727.

26. K. Spencer, D.M. Fabijanic, M.X. Zhang, Surf. Coat. Technol. 204 (2009) 336-344.

27. A. Shkodkin, A. Kashirin, O. Klyuev, T. Buzdygar, J. Therm. Spray Technol. 15(3) (2006) 382-386.

28. H. Koivuluoto, P. Vuoristo, J. Therm. Spray Technol. 19(5) (2010) 1081-1092.

29. J.M. Guilemany, J.M. de Paco, J. Nutting, J.R. Miguel, Metall. Mater. Trans. A 30 (1999) 1913-1921.

30. C. Verdon, A. Karimi, J.L. Martin, Mater. Sci. Eng. A 246 (1998) 11-24.

31. D.A. Stewart, P.H. Shipway, D.G. McCartney, Wear 225-229 (1999) 789-798.

32. L.M. Berger, S. Saaro, T. Naumann, M. Wiener, V. Weihnacht, S. Thiele, J. Suchánek, Surf. Coat. Technol. 202 (2008) 4417-4421.

33. E. Celik, O. Culha, B. Uyulgan, N.F. Ak Azem, I. Ozdemir, A. Turk, Surf. Coat. Technol. 200 (2006) 4320-4328.

34. H. Chen, C. Xu, Q. Zhou, I.M. Hutchings, P.H. Shipway, J. Liu, Wear 258 (2005) 333-338.

35. K. Kumari, K. Anand, M. Bellacci, M. Giannozzi, Wear 268 (2010) 1309-1319.

36. G.C. Saha, T.I. Khan, J. Eng. Mater-Technol. ASME 133(4) (2011) DOI:10.1115/1.4004689.

37. J.M. Guilemany, S. Dosta, J.R. Miguel, Surf. Coat. Technol. 201 (2006) 1180-1190.

38. H. Liao, B. Normand, C. Coddet, Surf. Coat. Technol. 124 (2000) 235-242.

39. A.C. Bozzi, J.D.B. de Mello, Wear 233-235 (1999) 575-587.

40. L. Zhao, M. Maurer, F. Fischer, R. Dicks, E. Lugsheider, Wear 257 (2004) 41-46.

41. H. Henke, D. Adam, A. Koehler, R.B. Heimann, Wear 256 (2004) 81-87.

42. Q. Wang, Z. Chen, L. Li, G. Yang, Surf. Coat. Technol. 206 (2012) 2233-2241.

43. D.A. Stewart, P.H. Shipway, D.G. McCartney, Surf. Coat. Technol. 105 (1998) 13-24.

44. Y. Liu, Y. Qiao, J. He, E.J. Lavernia, T.E. Fischer, Metall. Mater. Trans. A 33 (2002) 159-164.

45. H. Wang, W. Xia, Y. Jin, Wear 195 (1996) 47-52.

46. T. Liyanage, G. Fisher, A. Gerlich, Wear 274-275 (2012) 345-354.

47. J. He, Y. Liu, Y. Qiao, T.E. Fischer, E.J. Lavernia, Metall. Mater. Trans. A 33 (2002) 145-157.

48. P. Chivavibul, M. Watanabe, S. Kuroda, K. Shinoda, Surf. Coat. Technol. 202 (2007) 509-521.

49. H. Holleck, Constitutional Aspects in the development of new Hard Metals, Plenum Press, New York, 1983, 849-861.

50. A.I. Gusev, A.S. Kurlov, Inorg. Mater. 42(2) (2006) 121-127.

51. V.A. Tracey, Int. J. Refract. Met. Hard Mater., 11(3) (1992) 137-149.

52. H.J. Kim, Y.G. Kweon, R.W. Chang, J. Therm. Spray. Technol. 3(2) (1994) 169-178.

53. S. Hazra, K. Sabiruddin, P.P. Bandyopadhyay, Surf. Eng. 28(1) (2012) 37-43.

54. G. Di Girolamo, L. Pilloni, G. Pulci, F. Marra, J. Am. Ceram. Soc. 92(5) (2009) 1118-1124.

55. G. Di Girolamo, F. Marra, G. Pulci, J. Tirillò, T. Valente, L. Pilloni, Int. J. Appl. Ceram. Technol. 10(1) (2013) 60-71.

56. P. Chivavibul, M. Watanabe, S. Kuroda, J. Kawakita, M. Komatsu, K. Sato, J. Kitamura, J. Therm. Spray Technol. 17(5-6) (2008) 750-756.

57. P. Chivavibul, M. Watanabe, S. Kuroda, J. Kawakita, M. Komatsu, K. Sato, J. Kitamura, J. Therm. Spray Technol. 19(1-2) (2010) 81-88.

58. M.M. Khruschov, Wear 28 (1974) 69-88.

59. K. Jia, T.E. Fischer, Wear 200 (1996) 206-214.

60. F. Vargas, H. Ageorges, P. Fournier, P. Fauchais, M.E. López, Surf. Coat Technol. 205 (2010) 1132-1136.

61. D.H. Jeong, U. Erb, K.T. Aust, G. Palumbo, Scr. Mater. 48 (2003) 1067-1072.

62. M. Kouzeli, A. Mortensen, Acta. Mater. 50 (2002) 39-51.

63. R.S. Lima, B.R. Marple, Mater. Des. 29 (2008) 1845-1855.

64. G.E. Kim, J. Walker, J. Therm. Spray Technol. 16(1) (2007) 34-39.

65. ASTM E384, Standard Test Method for Knoop and Vickers Hardness of Materials, West Conshohocken, USA, 2011.

66. ASTM C1327, Standard Test Method for Vickers Indentation Hardness of Advanced Ceramics, West Conshohocken, USA, 2008.

67. ASTM G65, Standard Test Method for Measuring Abrasion Using the Dry Sand/Rubber Wheel Apparatus, West Conshohocken, USA, 2010.

68. Properties of Pure Metals, Properties and Selection: Non-ferrous Alloys and Special-Purpose Materials, ASM Engineered Materials Handbook, Vol. 2, ASM International, 1995, 1099 – 1201.

69. W.Y. Li, C. Zhang, X.P. Guo, G. Zhang, H.L. Liao, C.J. Li, C. Coddet, Mater. Des. 29 (2008) 297-304.

70. C.-J. Li, W.-Y. Li, Surf. Coat. Technol. 167 (2003) 278-283.

71. W.F. Smith, J. Hashem, Foundations of Materials Science and Engineering, fourth ed., McGraw-Hill, New York, NY, 2006.

72. ASTM E140, Standard Hardness Conversion Tables for Metals Relationship Among Brinell Hardness, Vickers Hardness, Rockwell Hardness, Superficial Hardness, Knoop Hardness, and Scleroscope Hardness, West Conshohocken, USA, 2007.

73. D. Goldbaum, J. Ajaja, R.R. Chromik, W. Wong, S. Yue, E. Irissou, J.G. Legoux, Mater. Sci. Eng. A 530 (2011) 253-265.

74. J. Ajaja, D. Goldbaum, R.R. Chromik, Acta. Astro. 69 (2011) 923-928.

75. J. Taylor, An Introduction to Error Analysis: The Study of Uncertainties in Physical Measurements, University Science Books, Mill Valley, CA, 1982, p. 89.

76. S.W.H. Yih, Tungsten: Sources, Metallurgy, Properties, and Applications, Plenum Press, New York, NY, 1979, p. 387.

77. A.T. Santhanam, P. Tierney, J.L. Hunt, Properties and Selection: Nonferrous Alloys and Special-Purpose Materials, *Cemented Carbides*, ASM Engineered Materials Handbook, Vol. 2, ASM International, 1990, 950-977.

78. B. Zahmatkesh, M.H. Enayati, Mater. Sci. Eng. A 527 (2010) 6734-6740.

79. R. Hill, Phys. Soc. –Proc. 65(389A) (1952) 349-354.

80. C.I. Chang, Y.N. Wang, H.R. Pei, C.J. Lee, J.C. Huang, Mater. Trans. 47(12) (2006) 2942-2949.

81. Q. Yang, T. Senda, A. Ohmori, Wear 254 (2003) 23-34.

82. H.S. Kim, Mater. Sci. Eng. A 289 (2000) 30-33.

83. D.C. Montgomery, Applied Statistics and Probability for Engineers, fourth ed., John Wiley & Sons, Hoboken, NJ, 2007. p 354-361.

84. S.M. Nahvi, P.H. Shipway, D.G. McCartney, Wear 267 (2009) 2083-2091.

85. Y. Morisada, H. Fujii, T. Mizuno, G. Abe, T. Nagaoka, M. Fukusumi, Surf. Coat. Technol. 204 (2010) 2459-2464.

86. H.-J. Kim, S.-Y. Hwang, C.-H. Lee, P. Juvanon, Surf. Coat. Technol. 172 (2003) 262-269.

7. Appendix

Hypothesis Tests on the Difference in Means for Matrix Hardness, Variances Unknown

Table 10: Statistics of the localized hardness of the matrix near carbides and away from carbides

	50WC matrix (*i* = 1)	**50WC matrix near carbide (*i* = 2)**
$\bar{x}_i$ ($HV_{0.01}$)	281	311
s_i ($HV_{0.01}$)	54	91
n_i	10	10

Assumptions:

- The population is normally distributed
- Unequal variances i.e. $\sigma_1^2 \neq \sigma_2^2$

Due to the low amount of samples taken, a t-test must be conducted.

Steps to determine if there is a statistical difference between the means:

1) We want to determine if $\mu_1 - \mu_2 = 0$
2) Therefore $H_o : \mu_1 - \mu_2 = 0 = \Delta_o$ or $H_o : \mu_1 = \mu_2$; hypothesis is true
3) $H_1 : \mu_1 \neq \mu_2$; hypothesis is false if $t_o^* < -t_{\alpha/2,\upsilon}$
4) Assume $\alpha = 0.05$ for 95% confidence
5) We must find the critical *t*-stat:

$$t_o^* = \frac{\overline{x_1} - \overline{x_2} - \Delta_o}{\sqrt{\frac{s_1^2}{n_1} + \frac{s_2^2}{n_2}}} = \frac{281 - 311 - 0}{\sqrt{\frac{54^2}{10} + \frac{91^2}{10}}} = -0.897$$

6) We must determine the appropriate degrees of freedom, rounded down to the nearest integer [83], by pooling the sample variances and sample sizes using the following equation:

$$\upsilon = \frac{\left(\frac{s_1^2}{n_1} + \frac{s_2^2}{n_2}\right)^2}{\frac{\left(s_1^2 / n_1\right)^2}{n_1 - 1} + \frac{\left(s_2^2 / n_2\right)^2}{n_2 - 1}} = \frac{\left(\frac{54^2}{10} + \frac{91^2}{10}\right)^2}{\frac{\left(54^2 / 10\right)^2}{10 - 1} + \frac{\left(91^2 / 10\right)^2}{10 - 1}} = 14.6 \approx 14$$

Therefore, $t_{\alpha/2,14} = 2.145$

Reject if $t_o^* > t_{\alpha/2,\upsilon} \rightarrow 0.897 < 2.145$; cannot reject our hypothesis, therefore our hypothesis is true, there is not enough evidence to suggest that there is a statistical difference between the two local matrix hardness values.